ELSEVIER

Biochimica et Biophysica Acta 1273 (1996) 108–128

BBA Biochimica et Biophysica Acta

Electronic structure of the oxidized primary electron donor of the HL (M202) and HL (L173) heterodimer mutants of the photosynthetic bacterium *Rhodobacter sphaeroides*: ENDOR on single crystals of reaction centers

M. Huber [a], R.A. Isaacson [b], E.C. Abresch [b], D. Gaul [c], C.C. Schenck [c], G. Feher [b,*]

[a] *Freie Universität Berlin, Fachbereich Chemie Institut für Organische Chemie, 14195 Berlin, Germany*
[b] *Department of Physics, 0319, University of California, San Diego, 9500 Gilman Drive, La Jolla, CA 92093-0319, USA*
[c] *Department of Biochemistry, Colorado State University, Fort Collins, CO 80523, USA*

Received 26 May 1995; accepted 18 September 1995

Abstract

The electronic structure of the primary electron donor (D) in the heterodimer mutants mutants HL (M202) and HL (L173) of the photosynthetic bacterium *Rhodobacter sphaeroides* was investigated using EPR and ENDOR (electron nuclear double resonance) methods on single crystals of reaction centers. In the mutants, one of the two bacteriochlorophyll (BChl) molecules of D is replaced by a bacteriopheophytin. The assignment of the ENDOR lines to specific methyl and non-methyl protons was accomplished by comparing the directions of the principal axes of the hyperfine tensors with the directions predicted from the X-ray structure and theory. We showed that the unpaired electron is localized on the BChl in the heterodimers, i.e., on the L-side (D_L) in the HL (M202) and on the M-side (D_M) in the HL (L173) mutant. Significant differences in the electronic structure of D_L and D_M were observed; they are attributed to the protein and/or pigment environment. Possible consequences of these differences for electron transfer, e.g., unidirectionality are discussed. The inequivalence of D_L and D_M also shows up in the asymmetry of the electronic structure of D in the native homodimer, whose electronic structure was reinterpreted using the heterodimers as monomer models.

Keywords: Electron transfer; Reaction center; Sequential mechanism; Structure; Electron donor; ENDOR; (*Rb. sphaeroides*)

1. Introduction

The primary electron donor D in bacterial photosynthetic systems is a dimer (special pair) of bacteriochlorophyll (BChl) molecules. The arrangement of the two BChl molecules, obtained from X-ray crystallography on *Rhodobacter sphaeroides* (*Rb. sphaeroides*) [1–7] is shown in Fig. 1. Details of the electronic structure of the cation radical of D^+ were investigated using EPR and ENDOR (electron nuclear double resonance) methods [8–10]. The unpaired electron in D^+ was found to be delocalized over both BChl molecules (D_L and D_M). The spin density distribution is asymmetric with a ratio of 2:1 in favor of D_L [11]. Models for the interaction of the dimer halves, the delocalization [8–10] and the origin of the asymmetry have been discussed [12].

A mutation in which one BChl of D is replaced by a bacteriopheophytin (BPh) alters the electronic structure resulting in the so-called heterodimer mutants [13,14]. This modification is achieved by replacing the histidines, which are close to the Mg atoms of D_L or D_M, by leucines using site-directed mutagenesis. In *Rb. sphaeroides*, either the histidine at position M202 or L173 is replaced by a leucine, resulting in the HL (M202) or HL (L173) mutant, respectively [14]. The composition of D in the mutants was confirmed by pigment extraction and metal analysis [14]. X-ray crystallography on the mutants [15] revealed the loss of a Mg atom at the appropriate position in both mutants. The structure of the HL (M202) mutant was solved, show-

* Corresponding author. Fax: +1 619 5340173.

SSDI 0005-2728(95)00134-4

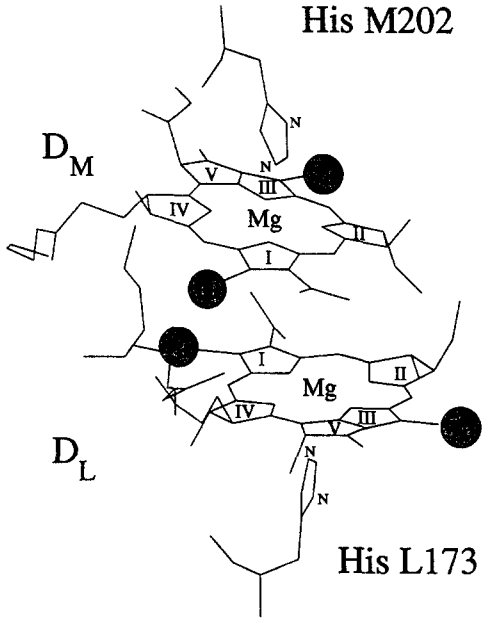

Fig. 1. Structure of the primary electron donor D in *Rhodobacter sphaeroides*. The phytyl side-chain has been partially truncated. In the heterodimer mutants HL (M202) and HL (L173) the histidines shown are replaced by leucines. As a result of the mutation, BChl at D_M (HL (M202)) and BChl at D_L (HL (L173)) are each replaced by a bacteriopheophytin. Coordinates: Brookhaven entry 1PSS [15].

ing that most of the differences between the atomic coordinates of the mutant and native RCs are within the resolution of the structures [15].

EPR/ENDOR methods are ideally suited to investigate the electronic properties of D^+ by measuring the hyperfine (hf) interaction of the unpaired electron with nearby magnetic nuclei. The hf interactions provide a sensitive way of obtaining molecular orbital (MO) coefficients of the orbital of the unpaired electron.

EPR and ENDOR/TRIPLE (electron nuclear triple resonance) measurements on D^+ of both heterodimer mutants in solution [16] showed that the unpaired electron is localized on one half of the dimer [1]. Information on the assignment of isotropic hyperfine coupling constants (hfc's) to individual protons was however limited. In the present work measurements on single crystals of reaction centers of both heterodimer mutants are reported, allowing a detailed assignment of hfc's to the protons in the molecule (see shaded protons in Fig. 2). In particular, we are able to assign hfc's to D_L or D_M and thereby determine on which of the chromophores the unpaired electron is localized. Preliminary accounts of this work have been reported in [18,19]. It was shown earlier that the electronic structure of D^+ of the two mutants is different [16], suggesting that the protein and/or pigment environment changes the electronic structure of the BChl's depending on whether they are situated at D_L or D_M.

The electronic structure of D^+ in R-26, the 'native' [2] system, has been investigated in a related study [11]. In the present study an independent assignment of hfc's to D_L and D_M in R-26 is given. Some of the questions concerning the electronic structure of D in the native system are: What is the molecular origin of the 2:1 asymmetry of D^+? What are the functional implications of the asymmetry? Can we place limits on the strength of the electronic coupling between the dimer halves? These questions have been addressed in part in the present study of the heterodimers.

With respect to functional implications, the electronic structure of D is discussed as a factor in controlling electron transfer properties of native RC's [20]. In particular, the asymmetry of the excited singlet state of D is invoked as a possible source of the 'unidirectionality', i.e., the preferred electron transfer along the A branch of the two quasi-symmetric pigment branches in the RC [20]. We discuss how the differences in the electronic structure of D in the heterodimers and in R-26 correlate with electron transfer properties, and, in particular, how the asymmetry of the electronic structure of the heterodimers affects electron transfer.

2. Materials and methods

2.1. Preparation and crystallization of RC's

The mutagenesis system employed to introduce the mutations is described in Ref. [14]. HL (M202) and HL (L173) mutant bacteria were grown as described [21]. The mutants are derived from the wild-type strain WS 231, a carotenoid containing strain. WS 231 is expected to be similar to the carotenoid containing wild-type strain 2.4.1., for which the X-ray structure has been determined [15], and whose structure we use in this work. Isolation and purification of RC's was done according to Ref. [22], with the modifications as described in Ref. [23].

RC's were crystallized as described in Ref. [3]. The heterodimer crystals were morphologically similar to those of R-26, i.e., needle-like with a length of approx. 4 mm and 0.5 mm at the widest dimension. The crystals had the same space group ($P2_12_12_1$) as those of R-26 [2–4]. The unit cell dimensions were within 1% of those of R-26 (a = 131.0 Å, b = 77.5 Å, c = 141.8 Å [2–4]), suggesting that the arrangement of the RC's in the unit cell system is the same. X-ray diffraction analyses on these mutants showed the absence of Mg in one of the BChl's of the

[1] EPR experiments on D^+ of similar mutation in *Rb. capsulatus* at the M200 site (equivalent to M202 in *Rb. sphaeroides*) were interpreted in a similar way [17].

[2] R-26 is a mutant strain of *Rb. sphaeroides* lacking the carotenoid. Otherwise (in particular with respect to the electronic structure of D) it is essentially indistinguishable from the native system.

dimer, but showed no other major structural changes [15]. The diffraction pattern of the crystals used in the ENDOR experiments was checked with a precession camera. The HL (M202) crystals diffracted to 3.5 Å, the HL (L173) crystals diffracted somewhat worse, but all crystals used in this work diffracted to at least 4 Å.

2.2. Instrumentation

EPR and ENDOR/TRIPLE spectra were recorded on a spectrometer of local design [24]. For ENDOR/TRIPLE measurements on single crystals, a dielectric resonator (DR) [25] was developed to replace the standard TM_{110} ENDOR cavity, thereby improving the spectrometer sensitivity for small samples. This was of particular importance for the heterodimer single crystals, since they were smaller than the R-26 crystals investigated previously [11,26,27]. The DR material (microwave ceramic Ba(Zr, Zn, Ta)O_3 was similar to that recommended by Walsh and Rupp [28] and by Dykstra and Markham [29]. The DR resonator was found to be mechanically more stable than a loop-gap resonator and had a much lower ENDOR background (Isaacson, unpublished). Although there were EPR background signals observed even in the best DR material tested, there were no detectable ENDOR background signals. The loaded Q with a typical aqueous protein crystal was about 1000. A 7-turn, 1 cm high by 1 cm diameter ENDOR coil acted as the primary shield for a stacked pair of dielectric rings (6.0 mm o.d. × 5.7 mm high) having a 3 mm hole. Microwave coupling was achieved via a Gordon coupler [30] feeding a box-like secondary shield containing a prism and a light pipe. For temperature control, a modified Varian V4557 gas flow system was used. Sample preparation and illumination for recording spectra of RC's

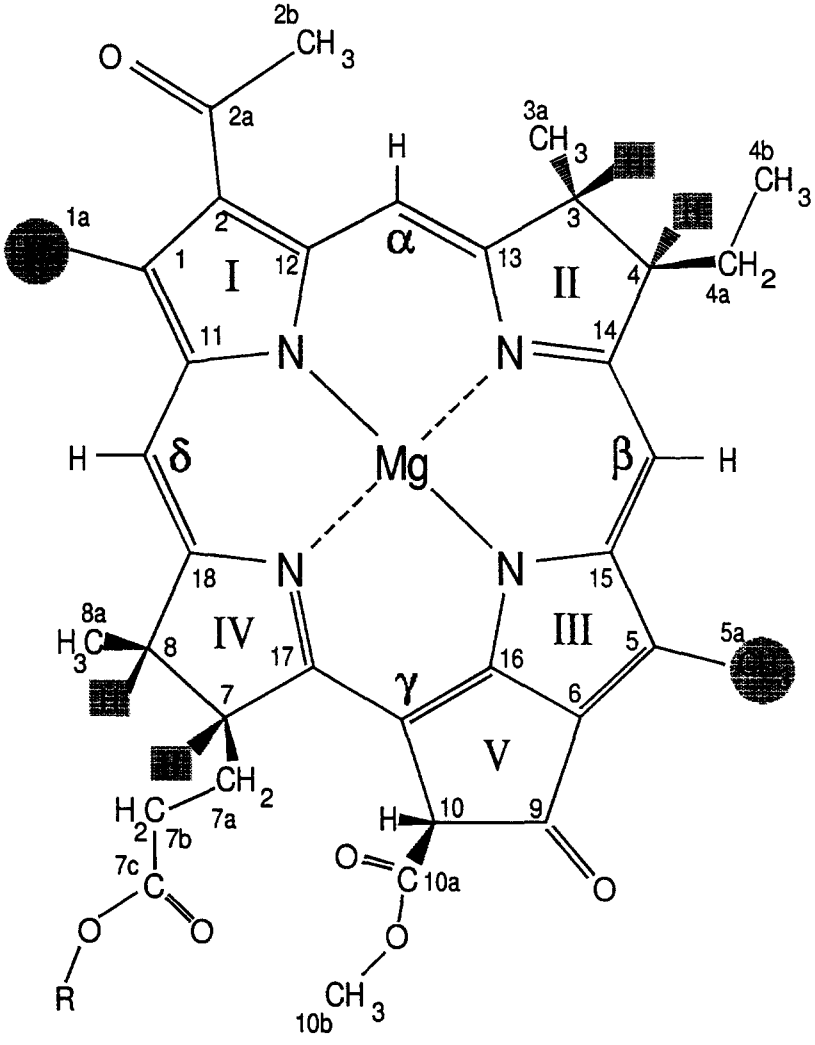

Fig. 2. Molecular structure and numbering scheme of BChl *a*. The β-protons of the methyl groups *1a* and *5a*, and the non-methyl β-protons at positions *3*, *4*, *7* and *8* were investigated in detail; they are shown shaded. Note that in the BChl dimer (Figs. 1 and 7) the fronts of the two BChl's, as shown in this figure, face each other.

in solution were as described earlier [16]. The liquid solution spectra were analyzed using a computer deconvolution program [31].

2.3. Crystal mounting and alignment

For measurements with the static magnetic field (B_0) in the ab-plane, in which the long axis of the crystal is perpendicular to B_0, the crystals were mounted vertically in X-ray capillaries [26]. For measurements with B_0 in the planes containing the long axis of the crystal, low-dielectric-loss plastic (Rexolite 1422 from C-Lec Plastics, Beverly, NJ, USA) pedestals were constructed. The pedestals were sealed with a Rexolite cap to prevent the evaporation of the mother liquor (see Fig. 3a). The pedestals were grooved to align the crystals according to the known crystal morphology: the crystals are needle-shaped and have a diamond-shaped cross-section with included angles of 58° and 122°. A 122° V-shaped groove was used to support the crystal with the *ac*-plane horizontal and a 58° V-shaped groove for the *bc*-plane horizontal (see Fig. 3a). By rotating the pedestal about the vertical axis, the magnetic field direction was varied in the desired plane. ENDOR/TRIPLE spectra were recorded in 5° intervals.

2.4. Formation of D^+ in single crystals

The cation radical of D was created by illuminating the crystal inside the cavity (for details, see [16,26]). The presence of the ENDOR coil and the non-transparent DR rings made it necessary to illuminate the sample from below (see Fig. 3b). To obtain sufficient light on the surface of a crystal, mounted with the long axis (*c*-axis) vertical (i.e., with B_0 in the *ab*-plane), a prism and a light pipe (a short quartz tube) were used instead of a mirror. The 'light tube' provides a radial source of light close to the bottom of the resonator thereby illuminating the crystal from all sides. Using a tube rather than a rod also permits the sample holder to extend up to 1 cm below the bottom of the DR rings, which allows more flexibility with crystal mounting. To minimize undesirable microwave reflections caused by standard mirror coatings, an unsilvered prism was used with a backing sheet of 0.025 mm thick aluminized mylar. For measurements in the *ac*- and *bc*-planes, the lower surfaces of the pedestals were polished to serve as light pipes. With the long axis of the crystal horizontal for the *ac*- and *bc*-plane mounts, only the lower half of the crystal surface could be efficiently illuminated.

3. Results

3.1. EPR Spectra

The EPR spectra of D^+ in the heterodimer mutants in solution at room temperature exhibit an unresolved, inhomogeneously broadened line with $g = 2.0028 \pm 0.0001$ (HL (L173)) and $g = 2.0027 \pm 0.0001$ (HL (M202)). The peak-to-peak linewidth (ΔB_{pp}) is $\Delta B_{pp} = (1.33 \pm 0.03)$ mT (HL (L173)) and $\Delta B_{pp} = (1.25 \pm 0.03)$ mT (HL (M202)). Thus, the EPR linewidth for both heterodimers is larger than for D^+ in R-26 measured under comparable

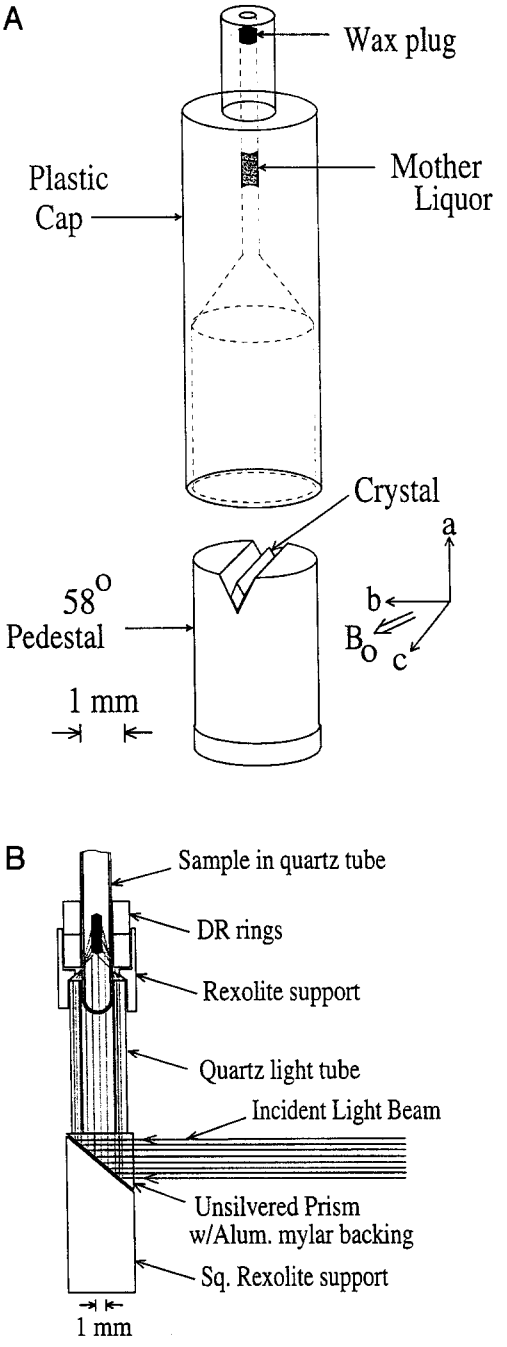

Fig. 3. Crystal mounts used for rotating the magnetic field B_0 in one of the principal crystallographic planes. (a) For the *ac*- and *bc*-planes, Rexolite pedestals were grooved to align the crystals. The pedestal used for the *bc*-plane is shown. (b) For the *ab*-plane and for liquid solutions, quartz capillaries were used as shown. To create D^+ the samples were illuminated from below with a mirror in (a) or with a light tube and prism in (b).

conditions ($\Delta B_{pp} = (0.95 \pm 0.03)$ mT). The linewidth of the heterodimers is similar to the linewidth of the monomeric BChl *a* cation radical (BChl a^+) in methanol/glycerol (1.28 ± 0.05) mT [32], suggesting localization of the unpaired electron on one half of the dimer.

In frozen solution, the linewidth of HL (L173) was measured to be (1.24 ± 0.05) mT [16], with a *g* factor of $g = 2.0032 \pm 0.0001$. The difference from liquid solution values is attributed to the presence of a small amount of free semiquinone anion radical (Q^-), whose signal is superimposed on D^+. In solution at room temperature, Q^- is presumably re-oxidized [33,34].

3.2. ENDOR and TRIPLE resonance spectra

3.2.1. General considerations

ENDOR/TRIPLE methods were used to resolve proton hyperfine (hf) splittings of the inhomogeneously broadened EPR line of D^+. In ENDOR spectra a pair of lines are observed for each hf coupling (A). The ENDOR resonance condition for nuclei with a spin of 1/2 is given by:

$$\nu^{\pm} = |\nu_n \pm \frac{1}{2}A| \quad (1)$$

where $\nu^{\pm}$ is the frequency of the ENDOR line and ν_n is the unperturbed nuclear Larmor frequency. To improve the ENDOR signal-to-noise ratio, the electron-nuclear-nuclear triple resonance method was used, in which both NMR transitions of a particular hf coupling (hfc) are irradiated simultaneously (special TRIPLE) [35,36]. The resulting spectra appear as ENDOR 'half spectra' (see Fig. 4). The amplitudes of the special TRIPLE lines are, under favorable relaxation conditions, proportional to the number of nuclei.

The relative signs of hfc's were determined from the generalized version (general TRIPLE) [37,38] of this experiment. In general TRIPLE, one NMR resonance is irradiated (pumped) continuously while the second rf field is swept as in ENDOR. This results in characteristic intensity changes of the ENDOR lines which reflect the

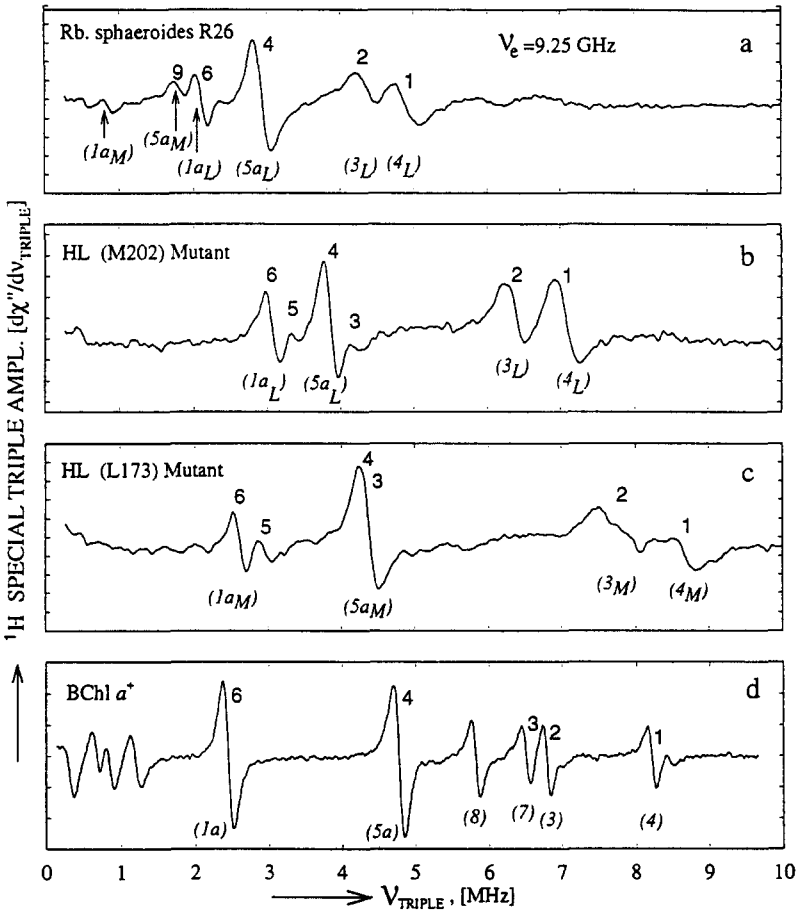

Fig. 4. Special TRIPLE spectra of D^+ in (a) R-26, (b) HL (M202), (c) HL (L173) and of (d) BChl a^+ in liquid solution. Line positions correspond to one half the hfc constants, *A*. Numbers in parentheses represent the assignments discussed in text. Values of the hfc's are summarized in the tables. Experimental conditions for panels a, b, c: $T = 288$ K; samples: $A_{800}^{1\,cm} = 33$, volume, 24 μl, TM_{110} cavity resonator, $Q_{LOADED} = 2500$, microwave power: (a) 50 mW, (b and c) 25 mW, (d). For experimental conditions see Ref. [42]. Rf power, 200 W (1.4 mT rot frame); rf frequency modulated at 15 kHz; modulation depth ± 100 kHz; averaging time (a) 80 min, (b) 4 h and (c) 7 h. Panels (a), (b), (c) modified from [16]; panel (d) modified from Ref. [42].

Table 1
Isotropic hyperfine coupling constants of D^+ in heterodimer mutants, R-26 and BChl a^+

Line [c]	HL (M202)			HL (L173)			R-26 [a]		BChl a^+ [b]	
	A_{iso} [d] [MHz]	A_{iso} [e] (MHz)	Assignment [f]	A_{iso} [d] (MHz)	A_{iso} [e] (MHz)	Assignment [f]	A_{iso} (MHz)	Assignment [f]	A_{iso} (MHz)	Assignment [f]
									−0.36	7a,4a
							1.24	$1a_M$	−0.51	8a
									+1.30	β,δ
9	−1.70(5)						3.19	$5a_M$	−1.64	10
8	+2.20(5)			1.90(5)						
7	+2.50(5)			2.80(5)					+2.34	α
6	+6.16(3)	+6.0	$1a_L$	+5.09(4)	5.1	$1a_M$	+4.06	$1a_L$	+4.93	1a
5	nr	6.6	8_L	nr	5.8	(8_M)			+11.76	8
4	+7.63(2)	+7.6	$5a_L$	+9.01(6)	8.6	$5a_M$	+5.58	$5a_L$	+9.62	5a
3	±8.26(3)	8.3	7_L	nr	10.0	(7_M)			+13.11	7
2	+12.82(4)	+12.8	3_L	16.00(12)	15.6	(3_M)	+8.58	3_L	+13.47	3
1	+14.16(3)	+14.2	4_L	17.70(11)	17.3	(4_M)	+9.59	4_L	+16.35	4

nr, not resolved; signs of hfc's obtained from general TRIPLE (see text); experimental errors in last digit shown in parenthesis. Assignments of hfc's in parentheses of HL (L173) were obtained in analogy with hfc's of HL (M202).
[a] Data from Lendzian et al. [11].
[b] In CH_2Cl_2/methanol, Data from Refs. [42] and [44] and H. Kaß et al., unpublished data.
[c] Line numbering according to Figs. 4, 6 and 9.
[d] From single crystal data: $A_{iso} = 1/3\,(A_{aa} + A_{bb} + A_{cc})$.
[e] From liquid solution spectra, errors: ±50 kHz.
[f] For numbering of protons, see Fig. 2.

relative signs of the hfc's [38]. Furthermore, if two types of radical are present or, as is the case for single crystals with magnetically inequivalent sites (see below), only lines belonging to the same radical or the same site will show intensity changes upon irradiating an NMR resonance of this radical.

3.2.2. ENDOR / TRIPLE of heterodimer RC's in solution

The hf interaction between the unpaired electron and magnetic nuclei consists of an isotropic part (the Fermi contact interaction, A_{iso}), which depends on the electron spin density at the nucleus and of an anisotropic part, A^{dip}, due to the dipole–dipole interaction. In liquid solutions the anisotropic part is averaged out and only the isotropic part of the hfc's is measured. In frozen solution (and in single crystals) both components of the hf interaction contribute to the observed hf splittings. The special TRIPLE spectra obtained for the heterodimer mutants in *liquid* solution are shown in Fig. 4. The center of the lines corresponds to one half of the isotropic hfc's (A_{iso}); the values are tabulated in Table 1. The hfc's are closer to those of the monomer, i.e., BChl a^+ in organic solvents (see Fig. 4d and Table 1), than to the homodimer D^+ in R-26 (Fig. 4a), indicating localization of the unpaired electron on one chromophore. This is analyzed more quantitatively in the Discussion section.

The ENDOR spectra of D^+ of the heterodimers in *frozen* solution have been studied previously (see Fig. 4 of Ref. [16]). In frozen solutions, well-defined powder patterns with relatively narrow linewidths are observed for the β-protons of rotating methyl groups (β-protons are protons which are separated by two bonds from the carbon atom carrying π-electron spin density). The ENDOR lines of the non-methyl β-proton hfc's, on the other hand, are broadened due to larger anisotropy. Using this linewidth criterion, lines 4 and 6 in the two heterodimer mutants are assigned to methyl protons. Furthermore, the powder patterns observed [16] confirm axial symmetry of the methyl

Table 2
Methyl proton hyperfine splittings of D^+ of the heterodimer in solutions and single crystals; $A_\parallel$, $A_\perp$ are parallel and perpendicular components of hf tensor

	Assignment	Liquid solution		Frozen solution [16]			Single crystals		
		Line	A_{iso}	$A_\perp$	$A_\parallel$	$1/3(2A_\perp + A_\parallel)$	$1/2(A_{xx} + A_{yy})$	A_{zz}	$1/3(A_{xx} + A_{yy} + A_{zz})$
HL (M202)	$1a_L$	6	6.0	5.6	(7.2)	6.1	5.57	7.36	6.16
	$5a_L$	4	7.6	7.0	8.4	7.6	7.08	8.72	7.63
HL (L173)	$1a_M$	6	5.1	4.7	6.1	5.2	4.62	6.03	5.09
	$5a_M$	4	8.6	8.1	10.0	8.7	8.41	10.17	9.00

For axially symmetric tensors: $A_{xx} = A_{yy} \cong A_\perp$ and $A_{zz} \cong A_\parallel$. For frozen solution $A_{iso} = 1/3(2A_\perp + A_\parallel)$; for single crystals $A_{iso} = 1/3(A_{xx} + A_{yy} + A_{zz})$.

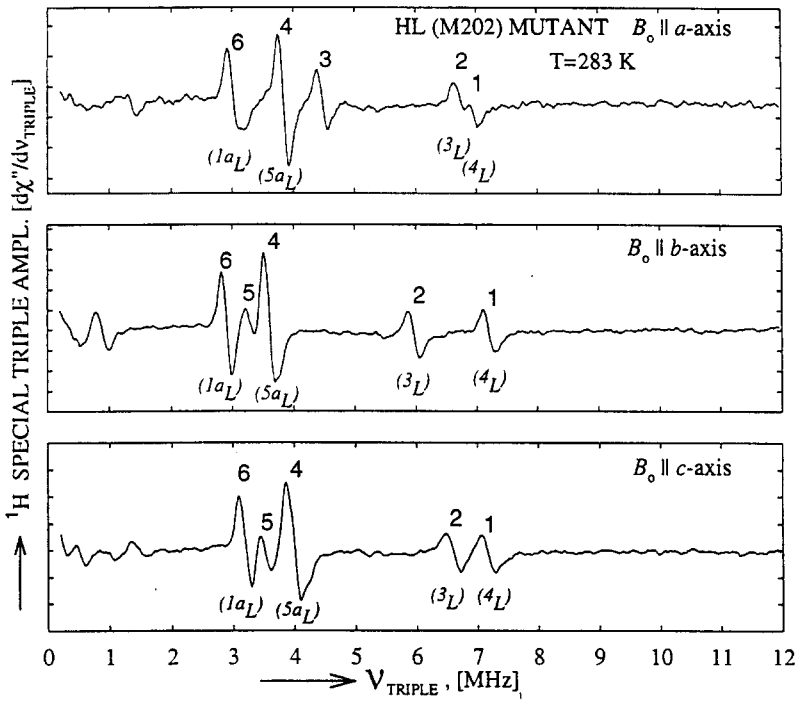

Fig. 5. Special TRIPLE spectra of D^+ in HL (M202) heterodimer single crystals. Spectra are shown for orientations with B_0 parallel to the crystallographic *a*-, *b*- and *c*-axes. A different crystal was used for each orientation. Line positions correspond to one-half the hfc constants, *A*. Numbers in parentheses represent the assignments discussed in text. Values of the hfc's are summarized in the tables. Experimental conditions: $T = 286$ K; dielectric resonator, $Q_{LOADED} \approx 1000$, microwave power: 0.25 mW; rf power 70 W (0.7 mT rot frame); rf frequency modulated at 15 kHz; modulation depth of ± 100 kHz; averaging time (a) 12 min, (b) 1 h and (c) 8 min.

group hf tensors (e.g., see Fig. 3 of Ref. [39]). The principal values obtained from the powder-patterns $A_{\parallel}$ (the parallel component corresponding to A_{zz}) and $A_{\perp}$ (the perpendicular component corresponding to $A_{xx} = A_{yy}$) are given in Table 2.

3.2.3. *ENDOR / TRIPLE of heterodimer RC's in single crystals*

Special TRIPLE spectra of D^+ in single crystals of RC's of the HL (M202) heterodimer mutant are shown in Fig. 5 for three orientations of the static magnetic field B_0 with respect to the crystallographic axes. The line positions change as a function of the orientation of the crystal in the field, due to the dipolar part of the hf interaction. In contrast to frozen solution spectra, where the dipolar hf interaction causes line broadening, the linewidths in single crystals are comparable to those observed in liquid solution spectra. Similar results were obtained for the HL (L173) mutant (data not shown).

The detailed angular dependence of the hf couplings, A, in the three principal crystallographic planes are shown for the two heterodimer mutants in Fig. 6. From an analysis of the data of Fig. 6, the hf tensors (**A**) for the nuclei in the crystallographic axis system were obtained. Diagonalization of **A** yields the principal values and axes of these tensors as described below.

The analysis of the angular dependence of the hf couplings was performed as described in [11]. The special TRIPLE resonance frequencies (ν_{ST}) are given by

$$2\nu_{ST} = A_{ii}\cos^2\theta + 2A_{ij}\cos\theta\sin\theta + A_{jj}\sin^2\theta \qquad (2)$$

where θ is the angle between B_0 and one of the crystallographic axes, A_{ii}, A_{jj} are the diagonal elements of the hf tensors in the crystallographic axis system and A_{ij} are the off-diagonal elements. Eq. (2) is valid as long as the hf interaction is small compared with the electron Zeeman interaction, the anisotropy of the *g*-tensor is small compared to the isotropic *g*-value, and the off-diagonal elements of **A** (A_{ij}) are small compared to A_{iso}.

The fits of the experimental data to Eq. (2) are shown as solid lines in Fig. 6. For several hf couplings, two

Fig. 6. Angular dependence of hf couplings of D^+ in the heterodimer mutant single crystals in the three principal symmetry planes. Hf couplings of (a) HL (M202) and (b) HL (L173) are plotted as a function of the angle, θ, of B_0 with respect to the crystallographic axes. Solid lines are fits to Eq. (2). Numbering of hf couplings as in Figs. 4 and 5. Assignments to specific protons given in italics. Two sets of lines for one hf tensor are due to the two magnetically inequivalent sites. Patterns are labelled □ or ○, depending on the sites to which they belong (obtained from general TRIPLE experiments as explained in text). The corresponding signs of A_{ij} follow from Eq. (3).

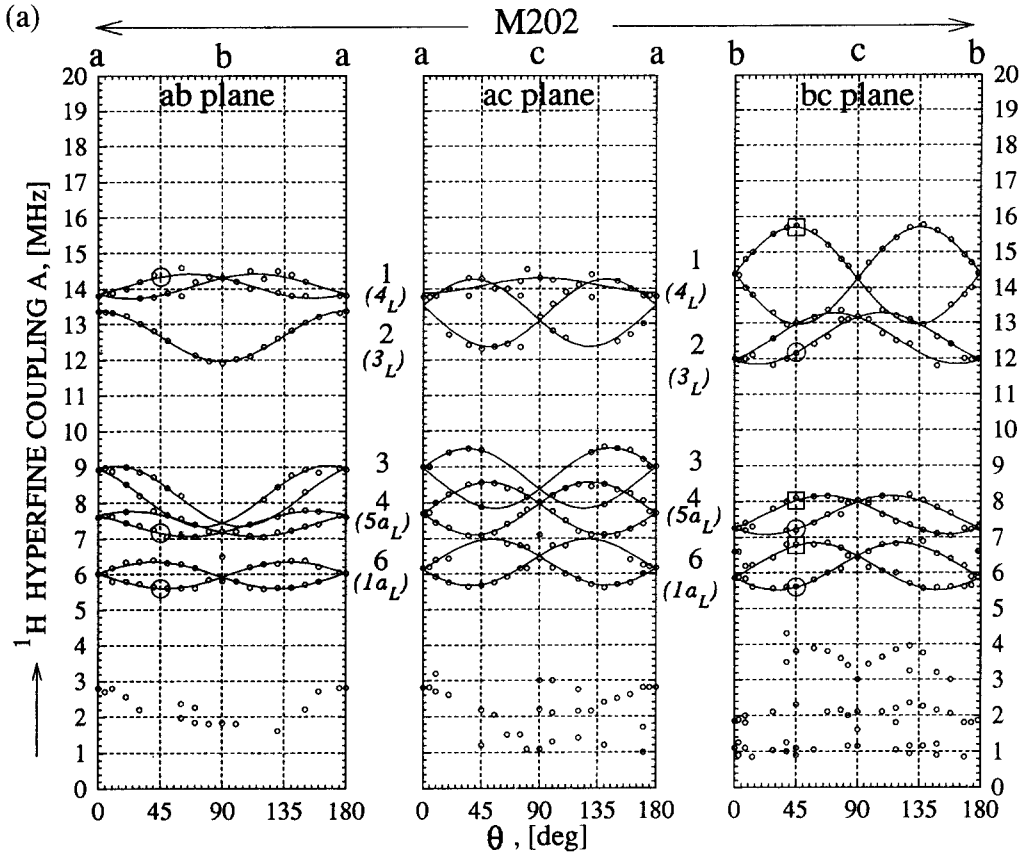
(a)
M202
a b a
a c a
b c b
ab plane
ac plane
bc plane
^{1}H HYPERFINE COUPLING A, [MHz]
1 (4_L)
2 (3_L)
3
4 ($5a_L$)
6 ($1a_L$)
θ, [deg]

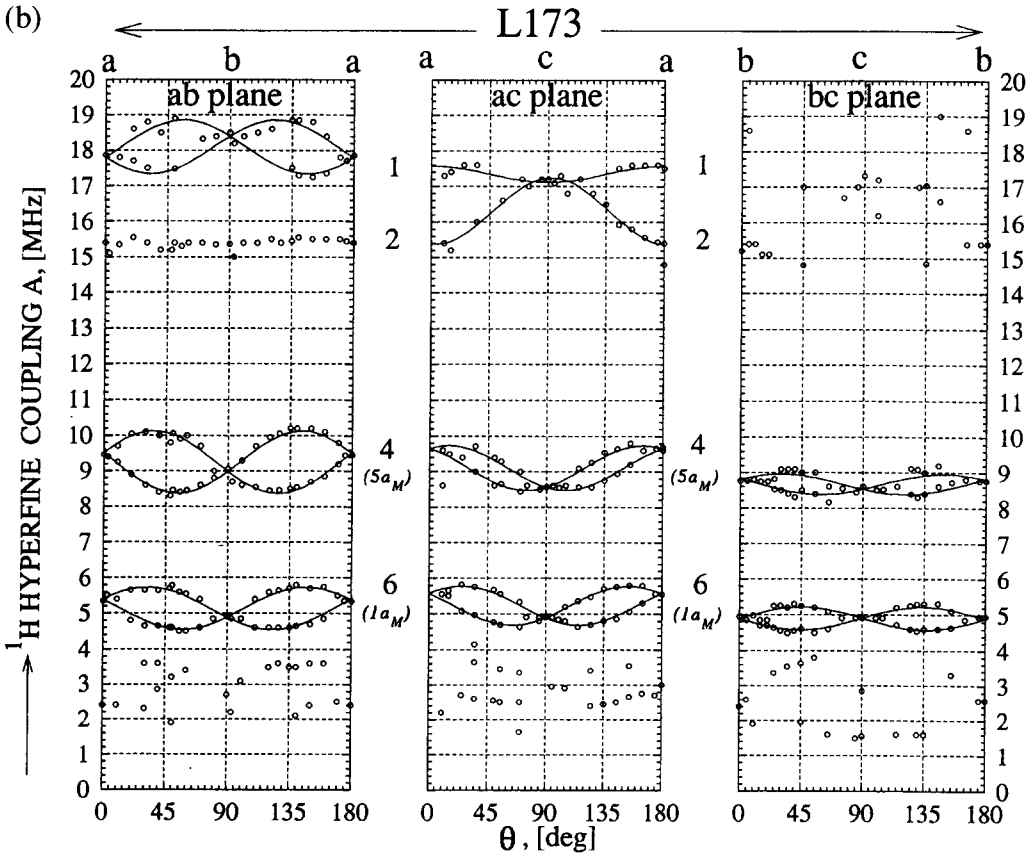
(b)
L173
a b a
a c a
b c b
ab plane
ac plane
bc plane
^{1}H HYPERFINE COUPLING A, [MHz]
1
2
4 ($5a_M$)
6 ($1a_M$)
θ, [deg]

Table 3
HF tensor elements A_{ij} in the crystallographic axis system (in MHz)

Line [a]	A_{aa}	A_{bb}	A_{cc}	A_{ab}	A_{ac}	A_{bc}
HL (M202) mutant						
1	+13.87(2)	+14.35(5)	+14.27(3)	−0.26(7)	±0.00(15)	+1.37(8)
2	+13.45(8)	+11.96(1)	+13.13(2)	±0.01(9)	±0.93(10)	+0.40(3)
3	+8.96(3)	+7.43(3)	+8.38(4)	±0.38(6)	±0.78(7)	nd
4	+7.68(2)	+7.22(4)	+7.98(1)	+0.26(6)	+0.72(3)	+0.40(5)
6	+6.09(6)	+5.89(3)	+6.49(1)	+0.38(9)	+0.63(7)	+0.59(4)
HL (L173) mutant						
1	+17.69(12)	+18.40(12)	+17.26(10)	±0.70(20)	0.00	nd
2	+15.39(12)	+15.40(12)	+17.24(12)	±0.00	0.00	nd
4	+9.58(7)	+8.90(9)	+8.55(2)	+0.84(16)	+0.32(9)	+0.25(11)
6	+5.48(9)	+4.89(1)	+4.91(1)	+0.54(10)	+0.43(10)	+0.32(2)

nd, not determined.
±, signs ambiguous or not determined.
[a] Numbering of lines according to Figs. 4, 5, 6.

curves that coalesce at the principal axes are observed. This 'site splitting' is due to the symmetry properties of the crystal. In the orthorhombic space group $P2_12_12_1$, corresponding to our crystals, there are four RC's, i.e., four sites, in the unit cell. The sites are pairwise equivalent (hence the two curves) when B_0 is in one of the crystallographic symmetry planes. All four sites are equivalent when B_0 is along a crystallographic axis (for details see [11]).

The elements of the hf tensors obtained from the fits are given in Table 3. The diagonal elements (A_{ii}) correspond to the hf couplings at the principal axes (see Fig. 5); their average values $\frac{1}{3}(A_{aa}+A_{bb}+A_{cc})$ correspond to A_{iso}. As shown in Table 1, these averages agree within experimental error with the values of A_{iso} measured in liquid solution. The off-diagonal elements (A_{ij}) are given by

$$2A_{ij} = A(\theta = 45°) - A(\theta = 135°) \quad (3)$$

To be able to diagonalize the tensor, the signs of the diagonal (A_{ii}) and the off-diagonal tensor elements (A_{ij}) are needed. A_{ii} is given by

$$A_{ii} = A_{iso} + A_{ii}^{dip} \quad (4)$$

Since the hf couplings analyzed have $A_{iso} > 0$ [11] and $|A_{ii}^{dip}| < |A_{iso}|$ (see Fig. 6), it follows from Eq. (4) that $A_{ii} > 0$.

The signs of the off-diagonal elements A_{ij} depend on the crystallographic site to which the hf tensor belongs. The relative signs of the off-diagonal elements of *different* hf tensors belonging to the same site were determined by using the general TRIPLE technique. Only lines of hf tensors belonging to the same site show intensity changes. Thus, pumping, for example, one of the resonances belonging to line 6 (marked by a square) in the *bc*-plane of the HL (M202) heterodimer (see Fig. 6a), caused intensity changes in the other lines marked by the same (square) symbol. These lines must, therefore, belong to the *same* crystallographic site as the pumped resonance. Since for all of them $A\ (45°) > A\ (135°)$, their signs according to Eq. (3) are positive. Using this information together with the additional knowledge of the absolute signs of A_{ij} of one hf tensor, the signs of the off-diagonal elements of the hf tensors were obtained as discussed in Appendix A.

For some tensors, either the signal-to-noise ratio of the spectra (e.g., lines 1 and 2 of HL (L173)) or the resolution (e.g., line 3 (see *bc*-plane of Fig. 6a) of HL (M202)) was not sufficient to determine all of the tensor elements, making the diagonalization impossible. In general, the signal-to-noise ratio of the spectra of the HL (L173) mutant was not as good as for the HL (M202). Consequently, only two hf tensors could be fully determined for HL (L173). The principal values of the hf tensors are given in Table 4.

The deviation of the hf tensors from axial symmetry (δ), is defined by

$$\delta = \left(A_{xx}^{dip} - A_{yy}^{dip}\right)/\left(A_{xx}^{dip} + A_{yy}^{dip}\right) \quad (5)$$

Their values are summarized in Table 4. Small values of δ associated with lines 4 and 6 of the two mutants are characteristic of methyl protons.

4. Assignment of hf couplings

The first question concerning the assignment is to determine on which half of D^+ the unpaired electron is localized. This question is addressed by using the directions of the principal axes of the methyl group hf tensors. (Later, the isotropic hfc's of these methyl groups are used as indicators of the electronic structure of D^+ (see Discussion).) We also discuss in this section the assignment of non-methyl β-protons, thus covering all nuclei having large isotropic hfc's (i.e., those with $A_{iso} > 3$ MHz).

Table 4
Principal values of diagonalized hf tensors

Mutant	Line [a]	Assignment	Principal values (A_{ii}^{dip}) of hf tensors [b] (MHz)			A_{iso} [c]	δ [d]
			A_{xx}^{dip}	A_{yy}^{dip}	A_{zz}^{dip}		
HL (M202)	1	4_L	−1.21(10)	−0.29(7)	+1.50(9)	14.16(3)	0.61(15)
	2	3_L	−1.12(5)	−0.33(10)	+1.48(11)	12.82(4)	0.54(16)
	4	$5a_L$	−0.60(5)	−0.50(5)	+1.09(4)	7.63(2)	0.09(10)
	6	$1a_L$	−0.65(6)	−0.54(6)	+1.20(8)	6.16(3)	0.09(12)
HL (L173)	4	$5a_M$	−0.67(6)	−0.50(6)	+1.17(6)	9.01(6)	0.15(12)
	6	$1a_M$	−0.54(7)	−0.40(7)	+0.94(7)	5.09(4)	0.15(17)

[a] Numbering of lines according to Fig. 6 and Tables 1 and 3.
[b] Principal values of diagonalized hf tensors, $A_{ii}^{dip} = A_{ii} - A_{i,\,i}$ (see Eq. (4)).
[c] Isotropic component of hf tensor.
[d] Deviation from axial symmetry defined as $\delta = (A_{xx}^{dip} - A_{yy}^{dip})/(A_{xx}^{dip} + A_{yy}^{dip})$. For an axially symmetric hf tensor $\delta = 0$, for maximum deviation from axial symmetry $\delta = 1$.

4.1. Assigning hf couplings to D_L or D_M

To determine whether the unpaired electron is localized on the chromophore on the L (D_L) or the M (D_M) side of D, the directions of the principal axes of the methyl group hf tensors are compared to the structure as follows: The dipole–dipole interaction of electron and nuclear spins for a rotating methyl group attached to a π-center (C_π) results in an axially symmetric hf tensor with the symmetry axis, i.e., the principal axis corresponding to the largest positive eigenvalue ($A_\parallel$ or A_{zz}) pointing approximately along the C_π–CH_3 bond. The direction of A_{zz} is then compared with the C_π–CH_3 bond direction determined from the X-ray structure.

In BChl *a* there are two methyl groups that are bound to π-electron centers (*1a* and *5a* in Fig. 2). Experimentally, the *1a* and *5a* methyl groups on one chromophore cannot be distinguished, since their C_π–CH_3 bond directions are nearly collinear. Studies on chlorophyll derivatives have shown that the *5a* methyl group has the larger isotropic hfc [40]. We therefore assign the methyl group with the larger A_{iso} to *5a*. The angles between the C_π–CH_3 bond directions of the methyl groups, obtained from the X-ray structure [15], and the principal axes, A_{zz}, were determined for all four sites: the ones with the smallest angle are summarized in Table 5. The proper assignment to D_L or D_M should give the best alignment (i.e., the smallest angles), as indicated by the bold numbers in Table 5.

For both methyl hf tensors of the HL (M202) mutant, the angles with the bond directions of D_L are smaller than those with D_M. Consequently, despite the relatively large

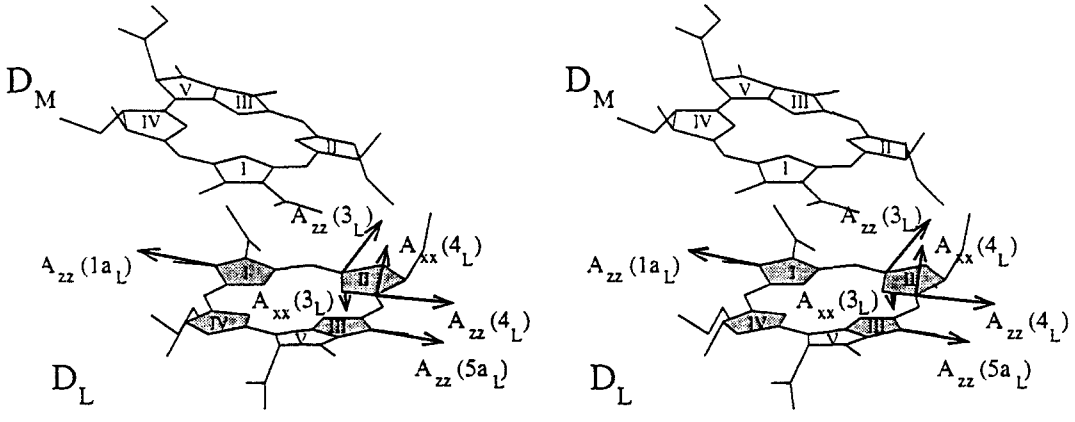

Fig. 7. Stereoview showing the orientation of the principal axes of the hf tensors of the HL (M202) mutant relative to the X-ray structure of D in wild type [15]. Shaded: pyrrole rings I through IV of D_L. Principal axes of hf tensors are shown as vectors. Vectors $A_{zz}(1a_L)$ and $A_{zz}(5a_L)$ are the principal axes of the largest eigenvalues of the hf tensors corresponding to lines 4 and 6 of the *1a* and *5a* methyl protons. Their directions are approximately collinear with the C_π–CH_3 bond directions. Vectors $A_{zz}(4_L)$, $A_{xx}(4_L)$ and $A_{zz}(3_L)$, $A_{xx}(3_L)$ are the principal axes of the hf tensors corresponding to lines 1 and 2 of the non-methyl β protons, shown with their origins at the corresponding C_π atom. $A_{zz}(4_L)$ and $A_{zz}(3_L)$ correspond to the largest (positive) eigenvalues, $A_{xx}(4_L)$ and $A_{xx}(3_L)$ to the smallest (negative) eigenvalues. $A_{zz}(4_L)$ and $A_{zz}(3_L)$ should point approximately along their respective C_π–H directions (see Appendix B and Fig. 11). Coordinates: Brookhaven entry 1PSS [15].

Table 5
Angles between principal axes of methyl hf tensors and C–CH_3 bond directions from the X-ray structure

	Methyl group	L-side [a]	M-side [a]
HL (M202)	*1a*	**9°**	14°
	5a	**11°**	28°
HL (L173)	*1a*	32°	**10°**
	5a	42°	**12°**

[a] Angles of principal axes of methyl group hf tensors with C–CH_3 bond of the crystallographic site that gives the smallest angle for each tensor (see text). X-ray coordinates (Brookhaven PDB entry 1PSS) from wild type (strain 2.4.1) [15].

angles between the bond directions and the principal axes (10° on the average [3]; the origin of this deviation is discussed below), these hf couplings are assigned to the methyl groups on D_L. In the case of the HL (L173) mutant, the angles with the bond directions of the methyl groups on D_M are smaller than with those of D_L (see Table 5). Consequently, they are assigned to methyl groups on D_M. Additional information is obtained by considering the orientation of the principal axes of the tensors relative to the BChl structure. For the pairs HL (L173)/D_M and HL (M202)/D_L, identical orientations are found. In particular, the axes of both hf tensors lie in the plane of the BChl, and the observed angle is due to a tilt from the bond direction within that plane (see Fig. 7 for the HL (M202)/D_L pair, where the tensor axes directions are labelled A_{zz} ($1a_L$) and A_{zz} ($5a_L$), respectively). The direction of the tilt relative to the neighboring C atoms is, in the case of the *1a* methyl group, a tilt away from C11 towards C2 (see Fig. 2), and for the *5a* methyl group away from C15 towards C6. The fact that this orientation is found in both mutants suggests that it is systematic rather than accidental. We attribute it to π-spin density close to the methyl groups. The spin density at C11 is larger than at C2 (and, similarly, larger at C15 than at C6, for the methyl group *5a*) [41]. Since the π-center carrying the larger spin density causes the tensor axis to tilt away from it (see also Appendix B) the directions of the observed tilts agree with theoretical predictions.

Thus, the unpaired electron in HL (M202) is localized on D_L and in HL (L173) on D_M, i.e., on the BChl's in the heterodimers [15]. This supports our earlier assignment [16] based on the lower oxidation potential of BChl relative to BPh, which causes the unpaired electron to be localized on the BChl chromophore in the heterodimer.

[3] Note that the deviations between bond directions and principal axes are larger than can be accounted for by the experimental errors of the principal axes of the hf tensors ($\pm 3°$ for the methyl hf tensors) and the X-ray structure ($\pm 4°$ [11]).

4.2. Assignment of non-methyl β-protons

The assignment of non-methyl β-protons is complicated by two factors: (i) The positions of protons, which are not given in the X-ray structure, are needed to compare the hf tensor directions with the molecular structure. The principal axis corresponding to the largest eigenvalue (A_{zz}) points approximately along the C_π–H direction of the C_π–C_β–H fragment (see Appendix B). Since the position of the proton in the fragment must be inferred from the atomic coordinates of the carbons, the directions obtained are less accurate than those of the C_π–CH_3 bond directions used for the methyl groups. (ii) Neighboring π-spin densities are expected to have relatively large effects on the directions of the principal axis. Model calculations (Appendix B) show that centers of π-spin densities in the vicinity of C_π can cause deviations of the tensor axes from the C_π–H directions of up to 30°.

The two factors discussed above make it difficult to analyze the directions of non-methyl β-proton hf tensors accurately. Fortunately, the *differences* in the orientations of the measured tensor directions are sufficiently large to decide between different assignments of the β-protons in question. The analysis is done for the HL (M202) mutant. In HL (L173), the corresponding tensors could not be completely determined, making an analysis of their orientations not possible.

For the hf tensors corresponding to lines 1 and 2 of the HL (M202) mutant (see Table 3), the signs of the off-diagonal elements were determined experimentally yielding the eigenvalues and the directions of the principal axes (see Appendix A). The tensors are non-axially symmetric ($\delta =$ 0.61 and 0.54, respectively, see Table 4 and Eq. (5)). For the hf tensor associated with line 2, the directions of two principal axes of this tensor relative to the molecular structure are shown in Fig. 7 (vectors labelled $A_{zz}(3_L)$ and $A_{xx}(3_L)$). $A_{zz}(3_L)$ corresponds to the largest, and $A_{xx}(3_L)$ to the smallest principal value (the justification of the assignment of line 2 to proton 3_L is discussed below). Note that experimentally one cannot distinguish between the directions of $A_{zz}(3_L)$ and $A_{xx}(3_L)$ as shown in Fig. 7 from those in which all three tensor components are inverted by 180°.

According to theory (Appendix B), A_{zz} should point approximately along the C_π–H direction. As seen in Fig. 2, proton *3* lies above the face of ring II of the BChl, whereas proton *4* lies below. In Fig. 7, where the 'face' of the BChl D_L is pointing up (same as Fig. 2), $A_{zz}(3_L)$ is pointing up, i.e., it is closer to the C_π–H direction of proton *3* than of proton *4*. However, the C_π–H direction of proton *7* of ring IV (see Fig. 2) is approximately collinear with that of proton *3* (the directions deduced from the structure differ by less than 10°). Consequently, line 2 is assigned to either proton *3* or proton *7*. In Fig. 7 the possible assignment of $A_{zz}(3_L)$ to proton *7* can be visualized by inverting the sense of $A_{zz}(3_L)$, and considering

that proton *7* lies below the plane of the BChl (Fig. 2). The analogous procedure for line 1 in Table 3 yields the principal axes $A_{zz}(4_L)$ and $A_{xx}(4_L)$ in Fig. 7. Although $A_{zz}(4_L)$ is closer to the plane of the BChl than $A_{zz}(3_L)$, it points below $A_{zz}(3_L)$ and is closer to the C_π–H direction of proton *4* than of proton *3*. Since the C_π–H directions of protons *4* and *8* are nearly collinear, line 1 is assigned to either proton *4* or *8*. The fact that $A_{zz}(4_L)$ is closer to the plane of the BChl than theory predicts (see Appendix B) may be due to experimental errors in determining $A_{zz}(4_L)$ or puckering of the π-electron system, not considered in the treatment in Appendix B.

To decide on the assignment, i.e., to distinguish between the two possible proton positions (i.e., *3* vs. *7* and *4* vs. *8*), we make use of the results obtained on BChl derivatives, which showed that protons *3* and *4* have larger isotropic hfc's than protons *7* and *8* [42]. We therefore assign line 1 to proton *4* and line 2 to proton *3*.

The hf tensor associated with line 3 could not be determined completely, because there is too much overlap with the lines of another hfc in one of the planes (the *bc*-plane, see Fig. 6a). The angular dependences of the hfc's in the remaining planes (the *ab*- and *ac*-planes) are similar to those of line 2 and significantly different from those of line 1 (compare Fig. 6a). This shows that the principal axes of the hf tensors associated with lines 2 and 3 must have similar orientations relative to the crystallographic axis system, i.e., they should be collinear. Since line 2 is assigned to proton *3*, line 3 should be assigned to proton *7*. Consequently, the smallest non-methyl β-proton hf tensor (see unlabeled points between 6 and 8 MHz in Fig. 6a) is assigned to proton *8* by default.

The non-axial symmetry of the β-proton hf tensors (see Table 4) is in agreement with calculations similar to those performed by McConnell and Strathdee [43] (Appendix B), which show that an additional center of π-spin density on a different carbon atom of the pyrrole ring (e.g., in the case of the β-proton *4*, C13, see Fig. 2) causes a deviation from axial symmetry. According to calculations, the principal axis corresponding to the smallest eigenvalue, i.e., the most negative one, should be perpendicular to the nodal plane of the π-electron system, as is observed experimentally (vectors labelled A_{xx} (4_L) and A_{xx} (3_L) in Fig. 7).

4.3. Simulations of the EPR line shape

A crucial test of the assignment of the hfc's is to check whether the multiplicities of the nuclei derived from the assignment, combined with the hfc's obtained from ENDOR, are consistent with the EPR line shape. This test is done by computer simulation of the liquid solution EPR spectra using the isotropic hfc's obtained by ENDOR. In the simulation of the EPR spectrum of D^+ of the HL (M202) mutant (see Fig. 8a) three protons were used for each of the methyl hfc's (lines 4 and 6), one proton for each of the non-methyl β-H hfc's (lines 1, 2, 3 and 5), and

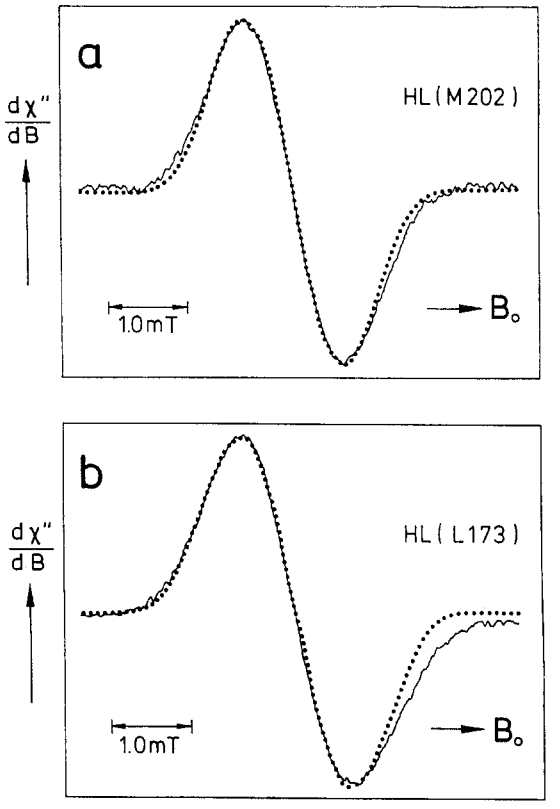

Fig. 8. Experimental (solid line) and simulated EPR spectra (dotted line) of D^+ in the heterodimer mutants in liquid solution, (a) HL (M202) and (b) HL (L173). For multiplicities and hfc's, see text. Gaussian single component lines with a width of 0.1 mT were used. The larger observed widths of the high field part of the experimental spectra are ascribed to incomplete averaging of the **g** and **A** tensors, resulting in asymmetric line broadening [45].

one for each of the smaller H hfc's (lines 7, 8 and 9) (see Table 1). Furthermore, four ^{14}N nuclei were included, using A_{iso} of 3.1, 2.9, 2.2, 2.2 MHz obtained for BChl a^+ given in [42,44].

For HL (L173) (see Fig. 8b) three protons were used for each of the methyl hfc's lines 4 and 6, and the ^{14}N nuclei were simulated with the same hfc's as used for the HL (M202) mutant. Of the non-methyl β-protons, one was assigned to each of the three hfc's having well resolved lines in the liquid solution special TRIPLE spectra (lines 1, 2, and 5), the fourth one to line 3. One proton was used for each small hfc (line 7 and 8) (see Table 1). The simulation gives additional evidence that the fourth non-methyl β-proton contributes to line 3 in the liquid solution special TRIPLE spectrum (see Fig. 4c). The two alternatives, simulated by assigning this proton to either line 2 or to a small hfc (< 3 MHz), result in significantly worse fits, and are therefore excluded. The fit of the low-field half of the line is very good, the deviation of the high-field side of the line is attributed to an incomplete averaging of the g and A tensors which results in an asymmetric line broadening [45]. We conclude that the simulations support the assignment given for both heterodimers. The multiplicities corre-

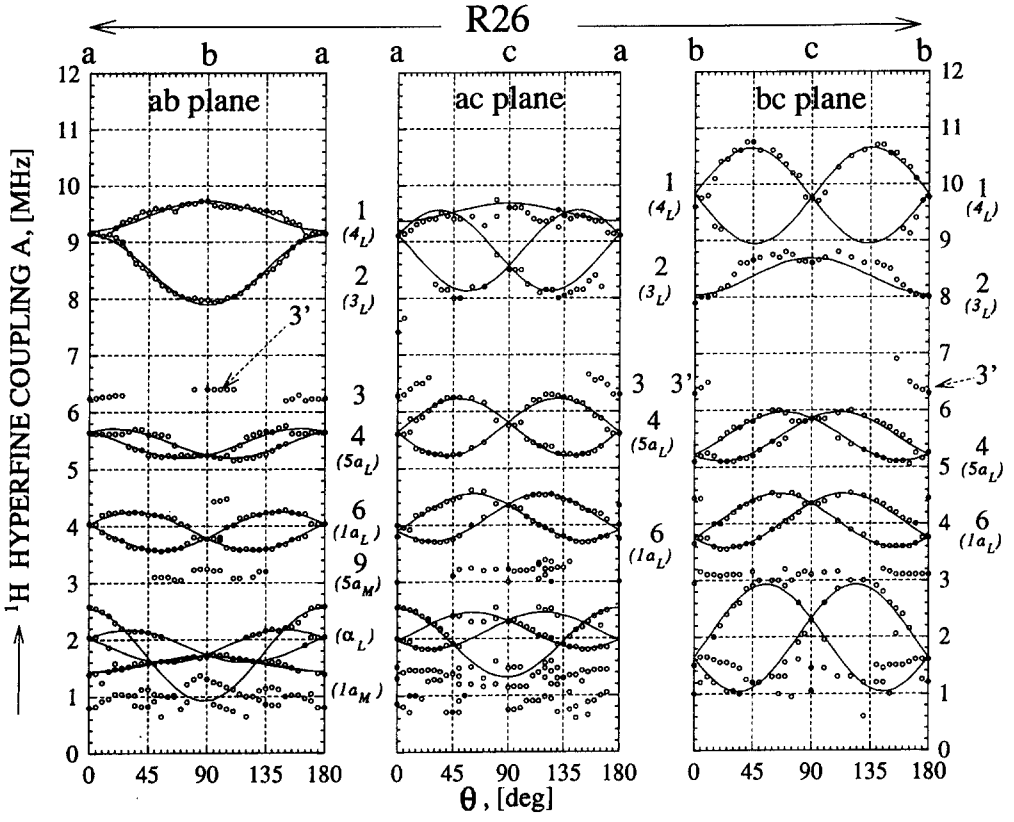

Fig. 9. Angular dependence of hf couplings of D^+ in R-26 single crystals (for experimental conditions see [11]). Hf couplings 1, 2, 4 and 6 have similar angular dependences as 1, 2, 4 and 6 in the HL (M202) mutant (Fig. 6a) and are therefore assigned to D_L. Line 3′ is not observed in the HL (M202) mutant (see Fig. 6a). This suggests that line 3′ is due to a proton on D_M.

spond to the number of nuclei on one BChl. Thus, there is no indication of an interaction with nuclei on the other chromophore.

4.4. Assignment of Hf couplings to D_L or D_M in R-26

The angular dependences of hf couplings of D^+ in single crystals of R-26 are shown in Fig. 9. The data shown are in agreement with those reported previously [11]. Since in R-26 the unpaired electron is delocalized over D_L and D_M, hf couplings to protons on both chromophores are expected. In order to determine whether hf couplings are due to protons on D_L or D_M their angular dependences are compared to the heterodimers. If the angular dependence of a hfc in R-26 is similar to HL (M202) it is assigned to D_L, if it is similar to HL (L173) it is assigned to D_M. The justification of this procedure is that the orientations of the respective chromophores (and hence the axes of the hf tensor components) of D in the crystals of R-26 and the heterodimers, as determined by X-ray diffraction, are the same [15]. As an example of the similarity in orientations of the hf tensors, the directions of the principal axes of the methyl hf tensors (lines 4 and 6) of D^+ in R-26 are compared to those of the heterodimers in Table 6. The directions of the principal axes in R-26 and HL (M202) are within 7° collinear, whereas the angles

Table 6
Angles between principal axes of methyl proton hf tensors of D^+ in R-26 and heterodimer mutants

Methyl group [a]	Line number in R-26 [b]	Angles between corresponding hf tensor principal axes A_{zz}					
		HL (M202)			HL (L173)		
		line [c]	assignment [d]	angle	line [c]	assignment [d]	angle
1a	6	6	$1a_L$	7°	6	$1a_M$	24°
5a	4	4	$5a_L$	7°	4	$5a_M$	35°

[a] Numbering of methyl groups according to Fig. 2.
[b] Numbering of hf tensors according to angular dependence of hf couplings in Fig. 9.
[c] Numbering of hf tensors according to Tables 3 and 4.
[d] Assignment from comparison of anisotropic hf couplings of D^+ in heterodimers with X-ray structure (see Table 5).

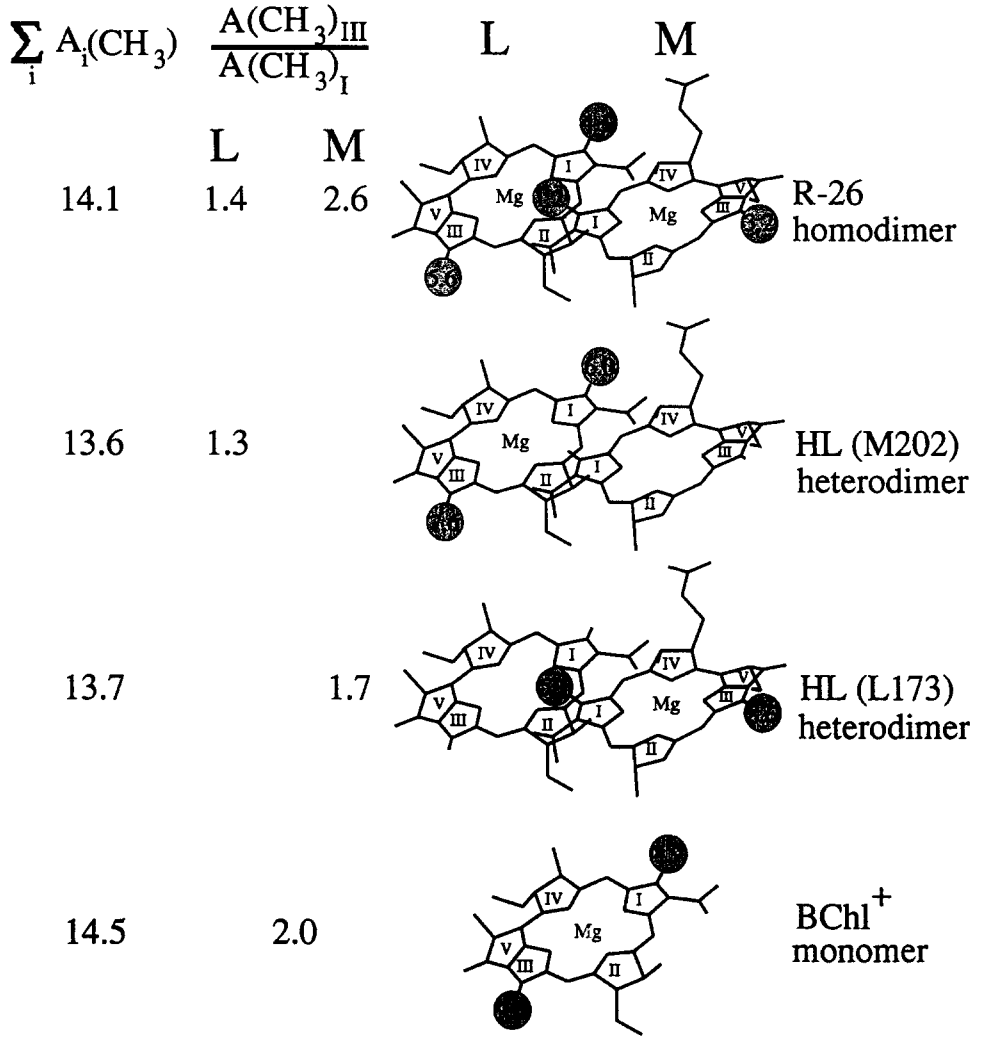

Fig. 10. Comparison of the isotropic hfc's of the CH_3 groups on rings I and III in the native homodimer the heterodimer mutants and the monomer $BChl^+$ showing the effect of environment on the spin density distribution (see Table 1). The sum of methyl hfc's ($\Sigma A_i(CH_3)$) is a measure of the total spin density; the ratio of *5a* and *1a* methyl hfc's ($A(CH_3)_{III}/A(CH_3)_I$) shows differences in spin density distribution in *one* chromophore. The assignments are from single crystal data of this work, and for the BChl a^+ from [42]. Modified from Ref. [18]

between R-26 and HL (L173) are significantly larger, thus confirming the assignment of lines 4 and 6 in R-26 to D_L. The angular dependences of lines 1, 2, 3, 4 and 6 in R-26 (Fig. 9) have an obvious similarity to lines 1, 2, 3, 4 and 6, respectively, in HL (M202) (Fig. 6a). Therefore, these lines are assigned to protons of D_L in D^+ of R-26. The partially resolved hfc line associated with 3′ in R-26 has no counterpart in the HL (M202) mutant. This hfc is therefore assigned to a proton on D_M in R-26, which has an hfc of $A_{iso} = 6.5 \pm 0.2$ MHz (from $A_{bb} = 6.5$ MHz, $A_{cc} = 7.2$ MHz (see Fig. 8 in Ref. [11]) and an estimated $A_{aa} = 6.0$ MHz).

The above results confirm the assignment given in Ref. [11], which was based on comparison with MO calculations. These MO calculations were required since in R-26 only two out of the four methyl group hf tensors were fully determined. The angles of the two tensors relative to the structure of D_L and D_M were too similar to allow an assignment.

5. Discussion

5.1. Localization of the unpaired electron in the heterodimers

5.1.1. Isotropic hyperfine coupling constants and spin densities

The largest isotropic hfc's of D^+ are due to β-protons. For β-protons the relation between the isotropic hfc (A_{iso}) and the π-spin density (ρ_π) at the nearest C_π atom is given by the Heller-McConnell relation [46]:

$$A_{iso} = \rho_\pi (A + B\cos^2\phi) \quad (6)$$

where A and B are empirical parameters and ϕ is the dihedral angle between the plane containing the C_π–C–H bonds and that containing the axis of the p_z orbital and the C_π–C bond. For protons of rotating methyl groups, the $\cos^2\phi$ term averages to 1/2, making A_{iso} directly proportional to the spin density. Thus, to compare spin densities, it is convenient to compare hfc's of methyl β-protons. There are two relatively large methyl hfc's in BChl a^+ (the *1a* and *5a* methyl groups, see Fig. 2), which are located at opposite ends of the π-system. They are used, therefore, as representative of the spin density distribution in the macrocycle. Fig. 10 summarizes the hfc's of the *1a* and *5a* methyl groups of the homodimer, the two heterodimers and the BChl a^+ monomer.

5.1.2. Degree of localization of the unpaired spin

The sum of the two methyl hfc's $\Sigma A_i(CH_3)$ is used as a measure of the total spin density on the macrocycle. Thus, the degree of localization of the unpaired electron in the heterodimers is obtained by comparing ΣA_i (CH_3) in the different systems (see Fig. 10). If the unpaired electron were fully localized on one chromophore, ΣA_i (CH_3) would be the same as in the isolated chromophore, BChl a^+. Any spin density on the other chromophore, i.e., on the BPh in the heterodimer, would reduce the spin density on the BChl, resulting in a reduction of ΣA_i (CH_3).

For both heterodimers $\Sigma A_i(CH_3)$ is only slightly smaller (by $\sim 5\%$) than $\Sigma A_i(CH_3)$ BChl a^+, indicating that most of the spin density is localized on the BChl half of the heterodimers. Similar results are obtained when comparing $\Sigma A_i(CH_3)$ in the heterodimers with the sum of all four methyl hfc's in D^+ of R-26.

The hfc's in the two heterodimers are significantly different from each other (see Fig. 10). These differences must be due to the local protein and/or pigment environments, which modify the electronic structure and conformation of the BChl's in the RC, as discussed in the following section.

5.2. Influence of the protein environment on the BChl's of D

The distribution of spin density in the BChl a^+ π-electron system is reflected in the ratio of the hfc's of the methyl groups at *5a* and *1a*, i.e., $A(CH_3)_{III}/A(CH_3)_I$. The observation is that on going from BChl a^+ to HL (L173) and HL (M202), progressively more spin density is shifted from ring III to ring I, as reflected in a decreasing ratio of $A(CH_3)_{III}/A(CH_3)_I$ (see Fig. 10). Since BChl a^+ in organic solvents is in a relatively nonperturbing environment the shift of spin density observed in the RC must be due to the protein and/or pigment environment of the BChl's. Two major factors account for the redistribution of spin densities [42,47,48]: (i) the orientation of the acetyl group at position 2 in ring I (Fig. 2) and (ii) hydrogen bonding to the carbonyl group at position 9 of ring V, and/or to the oxygen atom of the acetyl group. These two factors affect the spin densities as follows. (i) Rotating the acetyl group out of the plane of the porphyrin decreases the size of the π-electron system which, according to MO calculations [47,48], leads to an increase in the ratio $A(CH_3)_{III}/A(CH_3)_I$. For example, in BChl a^+, where $A(CH_3)_{III}/A(CH_3)_I$ is largest, the acetyl group is calculated to be almost perpendicular to the π-electron system [49]. (ii) A hydrogen bond to the acetyl group pulls spin density into ring I, thus decreasing $A(CH_3)_{III}/A(CH_3)_I$, whereas a hydrogen bond to the ring V keto group has the opposite effect, i.e., it pulls spin density into ring III, and thus leads to an increase in $A(CH_3)_{III}/A(CH_3)_I$.

The latter point was recently confirmed by ENDOR experiments on D^+ of a double mutant in which the heterodimer mutation HL (M202) is combined with a mutation (LH (L131)) designed to introduce a hydrogen bond at the keto group of ring V. The modification resulted in an increase of $A(CH_3)_{III}/A(CH_3)_I$ relative to HL (M202) [50,58] as predicted above.

Thus, the smaller $A(CH_3)_{III}/A(CH_3)_I$ ratio of HL (M202) compared to BChl a^+ could be either due to the acetyl group in D_L being more in the plane than in BChl a^+, or due to a hydrogen bond to the acetyl group. MO energy calculations on D^+ in R-26 suggest that the acetyl group of D_L is rotated out of plane, allowing the acetyl group to form a hydrogen bond to an amino acid residue (His L168) [12]. Such a hydrogen bond is also suggested in the structure described in [7]. According to the predictions stated above the two factors should have opposite effects. MO calculations on BChl a^+ using the RHF-INDO/SP method indicate that hydrogen bonding to the acetyl group is the dominant factor, reducing $A(CH_3)_{III}/A(CH_3)_I$, even if the acetyl group is rotated out of the plane by as much as 45° (Huber, M., unpublished data) which is the angle given in [12]. A mutation designed to break this hydrogen bond involves the replacement of His L168 by Phe. The corresponding heterodimer double mutant (HL (M202)/HF (L168)) shows indeed an increased $A(CH_3)_{III}/A(CH_3)_I$ ratio, relative to HL (M202) [50], thus supporting the conclusions arrived at above.

In the case of D_M, the ratio $A(CH_3)_{III}/A(CH_3)_I$ is larger than in D_L, but smaller than in BChl a^+. This suggests that either, the acetyl group is rotated out of the plane of the macrocycle, but not as far as in BChl a^+ or that a hydrogen bond to the keto group of ring V (see Fig. 2) exits. Neither suggestion finds strong support from other experimental evidence. Hydrogen bonding to the ring V keto group is unlikely, based on the results of vibrational spectroscopy [59] and X-ray crystallography [4–7]; the rotational angle of the acetyl group in the X-ray structures is approximately 15° [4–7]. We thus conclude that, whereas the effect of the protein/pigment environment on the spin density distribution of D_L can be adequately explained, the factors leading to the spin density distribution in D_M are not well understood.

The non-methyl β-proton hfc's of the heterodimers (lines 1, 2, 3 and 5 in Table 1) differ more strongly from those of BChl a^+ than the methyl proton hfc's. In particular, the two smaller non-methyl β-proton hfc's in the HL (M202) mutant (lines 3 and 5, assigned to protons *7* and *8* on ring IV) are reduced significantly (see Table 1). The smaller hfc's for the protons at ring IV are attributed to a larger angle ϕ (see Eq. (6)) which could be caused by a puckering of ring IV (twist of the C7–C8 bond to an orientation more perpendicular to the plane of the macrocycle, see Fig. 2) as has been suggested by Davis et al. [47]. In the HL (L173) mutant the same trend is observed as in HL (M202).

The fact that the two BChl's in the special pair are not identical, either to each other or to BChl a^+, in solution has some bearing on the interpretation of the electronic structure of D^+ in R-26, discussed in the next section.

5.3. The electronic structure of D^+ in R-26

The unpaired electron on D^+ in the homodimer of R-26 is delocalized over D_L and D_M. The spin density distribution over the two halves is asymmetric with a ratio of $\rho_L/\rho_M \cong 2$. To gain further insight into the electronic structure of the homodimer, we compare the spin density of each half with those of an appropriate model monomer. Since the electronic structure of the BChl's is affected by the protein environment, the appropriate monomers are the BChl's of the respective heterodimer mutant RCs and *not* the BChl a^+ monomer in solution. The results of the ratios of hfc's A_{DIM}/A_{MON} are summarized in Table 7, where for comparison we also quote the results on BChl a^+ in solution, although, as pointed out above, only the ratios using the heterodimers will be used. The following conclusions can be drawn from the values in Table 7.

(i) The reduction factors A_{DIM}/A_{MON} are not constant for all molecular positions, i.e., the wavefunctions do not scale.

(ii) The ratios A_{DIM}/A_{MON} at the individual positions within each half of the dimer are more similar on D_L than on D_M, i.e., the reduction factors scale for the positions on D_L, whereas they do not on D_M.

(iii) The ratios of the methyl hfc's $A(CH_3)_{III}/A(CH_3)_I$ discussed in the previous section are closer to the monomeric (heterodimer) ones in D_L (1.4 vs. 1.3) than in D_M (2.6 vs. 1.7) (see Fig. 10). This means that the wavefunction in the D_L dimer half of R-26 resembles the monomer wavefunction.

(iv) The average of the ratios A_{DIM}/A_{MON} on D_L is approximately twice as large as on D_M, reflecting the larger spin density on D_L

The overall conclusion of (i)–(iv) is that the two halves of the dimer are affected differently by the dimerization. Furthermore, points (ii) and (iii) show that the wavefunction of the D_L dimer half resembles the monomer wavefunction, whereas the wavefunction of D_M does not.

The above results can be accounted for by a simplified dimer model calculation presented by Plato [12]. He showed that for a small coupling of the dimer halves, the monomer wavefunctions remain unperturbed, resulting in an approximate scaling of the spin densities at the individual π-center positions for both dimer halves. For stronger coupling, the model predicts an approximate constant scaling factor for the spin densities on the dimer half with the higher spin density (i.e., D_L in our case) and a stronger perturbation of the monomer wavefunction of the dimer half with the smaller spin density (Plato, M., personal communication). This is in accord with points (ii) and (iii) above. The model further predicts that spin densities are pushed out of the overlap region, which in the dimer corresponds to rings I. Thus, the large reduction in the hfc at $1a_M$ results in the observed large ratio of $A(CH_3)_{III}/A(CH_3)_I$ on the M half (see Fig. 10), which is the half whose wavefunction is more perturbed (see point (iii)). The hfc results show that we have larger coupling between the dimer halves than originally postulated [12]. Thus, the dimer should be regarded as a supermolecule in which the molecular orbitals extend over the entire dimer.

Table 7
Comparison of isotropic hfc's in MHz in D^+ of R-26, the heterodimers HL (M202), HL (L173) and the monomeric BChl

Assignment	Isotropic hfc's (A_{iso}) of D^+			Ratios of hfc's (A_{DIM}/A_{MON})	
	R-26	HL(M202)	HL(L173)	(R-26)/ (heterodimer)	(R-26)/ (BChl a^+) [a]
$1a_M$	1.24(4)	–	5.09(4)	0.24(4)	0.25(3)
$5a_M$	3.19(4)	–	9.01(6)	0.35(4)	0.33(3)
$1a_L$	4.06(4)	6.16(3)	–	0.66(2)	0.82(2)
$5a_L$	5.58(4)	7.63(2)	–	0.73(1)	0.58(1)
3_L	8.58(5)	12.82(4)	–	0.67(1)	0.65(1)
4_L	9.59(5)	14.16(3)	–	0.68(1)	0.59(1)

[a] For hfc's of BChl a^+ see Table 1.
Ratios of the hfc's A_{DIM}/A_{MON} are listed for the heterodimer and BChl a^+ as monomeric references. Experimental errors in last digit shown in parentheses.

More subtle effects of the electron delocalization in D^+ of R-26 are found in the anisotropic part of the hf interaction. For the methyl proton tensors in D^+ of R-26 the deviation from axial symmetry δ (Eq. (5)) is greater than in the heterodimers (see Table 4). In particular, δ is larger for the $1a_L$ methyl group ($\delta = 0.41$) than for the $5a_L$ methyl group ($\delta = 0.17$) in R-26. [4] Since the $1a_L$ methyl group is closer to the overlap region of D_L and D_M than the $5a_L$ methyl group, the larger deviation from axial symmetry is likely to be caused by the proximity of centers of π-spin density on the other macrocycle.

5.4. The relation between spin density distribution and electron transfer rates

The electronic structure of D plays a role in the primary electron transfer steps in the RC. Specifically, preferential electron transfer along the pigments on the A branch of the protein (unidirectionality), has been attributed, at least in part, to the asymmetry of the electronic structure of D [20]. Since, in the present work, we measure the asymmetry of the electronic structure of D in the heterodimers, it is of interest to estimate how the difference in the electronic structure of D in the heterodimers and the wild type is expected to affect the electron transfer rates. To accomplish this, we calculate the effect of the change in electronic structure of D expected from the theory developed in [20].

Experimentally, the upper limit of the yield of ET to the bacteriopheophytin (ϕ) along the B-branch, is similar (10%) in the two heterodimers [14]. The ET rates along the A-branch are significantly smaller in the heterodimers than in wild type ($k_{ET} = 0.3$ ps^{-1} in wild type compared to $k_{ET} \cong 0.02$ ps^{-1} in HL (M202) and $k_{ET} \cong 0.01$ ps^{-1} in HL (L173)) [14].

The electron transfer rate k_{ET} is given by [51]

$$k_{ET} = \frac{2\pi}{\hbar} V_{DA}^2 FC \tag{7}$$

where V_{DA} is the electronic matrix element and FC is the Franck-Condon factor. The ratio of the electron transfer rates $k_{ET}(A)/k_{ET}(B)$ is proportional to the square of the ratio of the electronic matrix elements $[V_{DA}(A)/V_{DA}(B)]^2$. We shall focus on V_{DA}, which can be approximated by ([20,52]):

$$V_{DA} = KS_{DA} = K \sum_j \sum_k c_j^D c_k^A S_{jk}^{DA} \tag{8}$$

where K is a constant and S_{DA} is the intermolecular overlap integral which reflects: (i) the *electronic asymmetry* of the dimer through the molecular orbital coefficient c_j^D and (ii) the *structural differences* between the two dimer halves in relation to the acceptor through the overlap S_{jk}^{DA} of the atomic orbitals j and k.

Recent experiments [53] favor a sequential mechanism of electron transfer from D^* (the excited singlet state of D) to the bacteriopheophytin ϕ via the short-lived kinetic intermediate bacteriochlorophyll anion B^-, i.e., $D^*B\phi \xrightarrow{k_{DB}} D^+B^-\phi \xrightarrow{k_{B\phi}} D^+B\phi^-$, with k_{DB} dominating electron transfer, i.e., $S_{DA} \cong S_{DA}(DB)$. In the alternative single step, superexchange, mechanism [20], the state D^+B^- serves as an intermediate, virtual state. In this case, the energy difference between D^*B and D^+B^- as well as the overlap between B and ϕ ($S_{DA}(B\phi)$) needs to be considered (see Eq. 1.4 in [20]). We shall focus on the sequential mechanism and point out later the modifications required for the superexchange mechanism.

Electron transfer can proceed from both dimer halves D_L and D_M to B; consequently, S_{DA} has two terms: $S_{DA}(D_LB)$ and $S_{DA}(D_MB)$. To calculate the electron transfer asymmetry (unidirectionality) we need to evaluate the ratio

$$\left(\frac{V_{DA}(A)}{V_{DA}(B)}\right)^2 = \left(\frac{S_{DA}(D_LB_A) + S_{DA}(D_MB_A)}{S_{DA}(D_LB_B) + S_{DA}(D_MB_B)}\right)^2 \tag{9}$$

Values of $S_{DA}(DB)$ were calculated for *Rps. viridis* by Plato et al. [20]:

$$S_{DA}(D_LB_A) = 0.12 \cdot 10^{-4};\ S_{DA}(D_LB_B) = 0.23 \cdot 10^{-4}$$
$$S_{DA}(D_MB_A) = 1.02 \cdot 10^{-4};\ S_{DA}(D_MB_B) = 0.17 \cdot 10^{-4} \tag{10}$$

As seen from Eq. (10), electron transfer is dominated by $S_{DA}(D_MB_A)$. This is due to the smaller distance between D_M and B_A and the larger charge on D_M.

To calculate the unidirectionality expected for the two heterodimer mutants (assuming the sequential mechanism), we make the following, rather crude, assumptions: (i) the S_{DA} values calculated for *Rps. viridis* are applicable to *Rb. sphaeroides*; (ii) the contribution of the FC factor to unidirectionality is neglected; (iii) the spin localization in the heterodimer is 95% on D_M in HL (L173) and 95% on D_L in HL (M202); (iv) Eq. (9) can be simply modified for the heterodimer by taking into account the measured asymmetry in spin densities as described below.

We need to relate spin densities to electron densities, which are proportional to the molecular orbital coefficients c_j^D in Eq. (8) [54]. The spin densities in D^+ are measured in the highest occupied molecular orbital (HOMO), whereas the relevant orbital from which electron transfer occurs is the lowest unoccupied molecular orbital (LUMO). Fortunately, as shown by MO calculations on D, HOMO and LUMO coefficients on D_L and D_M are related to each other by a mirror image symmetry [20], e.g., large HOMO coefficients on D_L correspond to large LUMO coefficients on D_M. Neglecting spin spin polarization effects [54], we

[4] The values of δ were obtained from Eq. 5 and Table 2 of Ref. [11] (San Diego data).

can, therefore, relate the ratio of the molecular orbital coefficients $c_j^D(L)/c_j^D(M)$ to the ratio of spin densities ρ_L/ρ_M by:

$$\frac{c_j^D(L)}{c_j^D(M)} \cong \sqrt{\frac{\rho_M}{\rho_L}} \tag{11}$$

where we take for c_j^D and ρ averages over the whole molecule. For the heterodimers the S_{DA} values in Eq. (10) need to be modified using Eqs. (8) and (11) with a spin asymmetry of 20 rather than the 2.8 that was used for the *Rps. viridis* homodimer. For the HL (M202) mutant, for instance, this means that the second terms in the numerator and denominator of Eq. (9) need to be multiplied by $\sqrt{20/2.8}$. The values for $[V_{DA}(A)/V_{DA}(B)]^2$ for HL (M202) and HL (L173) obtained from Eqs. (9) are 18 and 1, respectively, as compared to 8 for the homodimer.

The above results predict that unidirectionality in the HL (M202) mutant should be enhanced, whereas in the HL (L173) mutant significant electron transfer (50%) should occur along the B-branch. The prediction concerning HL (M202) cannot be checked from the data given in [14], since only a lower limit of $k_{ET}(A)/k_{ET}(B)$ was measured. In HL (L173), electron transfer along the B-branch was not observed, suggesting that the predictions are off by at least a factor of 10 in the ratio $[V_{DA}(A)/V_{DA}(B)]^2$. A breakdown of any of the assumptions (i)–(iv) enumerated previously could account for this failure. A likely culprit is the neglect of the FC factor (assumption (ii)), which in view of the higher midpoint potential of the mutants (wild-type E_M: +0.50V; HL (M202) E_M: +0.66V; HL (L173), E_M: +0.68V) [55] should play a role. An increase in E_M reduces the driving force for charge separation, which in the normal region of the Marcus relation slows down electron transfer [56]. A detailed discussion of the energetics is given in [14,57].

Another possible explanation for this discrepancy is the effect of superexchange on the ratio of rates. To evaluate this effect the values for $[V_{DA}(A)/V_{DA}(B)]^2$ given above need to be multiplied by $[S_{DA}(B_A\phi_A)/S_{DA}(B_B\phi_B)]^2$ and the ratio of the energy denominators $[\Delta E_{DB}(B)/\Delta E_{DB}(A)]^2$ to obtain the electron transfer matrix element. The value for the ratios of $S_{DA}(B\phi)$ along the A- and B-branch was calculated to be ~ 4 [20], resulting in a preference of ET along the A-branch, i.e., a better agreement with the experimentally determined unidirectionality of the HL (L173) mutant. There is no consensus in the literature concerning the value of ΔE_{DB} for both branches. Consequently, it is difficult at present to estimate the contribution of superexchange.

In summary, the above results suggest that although the matrix element may play a role in contributing to unidirectionality, other factors may need to be considered. To obtain more meaningful comparisons between experiment and theory, it would be highly desirable to determine experimentally values, rather than limits, of the asymmetry of electron transfer.

6. Conclusions

The electronic structure of the cation radical of the primary electron donor in the BChl-BPh heterodimer mutants HL (M202) and HL (L173) has been characterized by EPR and ENDOR spectroscopy. The isotropic and anisotropic components of the proton hfc tensors were determined from the angular dependence of the hf couplings with respect to the external magnetic field. The assignment of the hf lines to specific protons was accomplished by comparing the directions of the principal axes of the hf tensors with the directions predicted from the X-ray structure and from theoretical considerations. Simulation of the EPR line shape confirmed the assignments.

The unpaired electron is localized on the BChl half of the heterodimer. This is consistent with the fact that BChl is easier to oxidize than BPh and is in agreement with previous assignments (e.g., Ref. [14]).

The hfc's of the two heterodimers differ significantly, reflecting differences in the electronic structures and conformations of the BChl's at D_L and D_M. The source of this difference is the different protein and/or pigment environment of D_L and D_M. For BChl at D_L the dominant interaction seems to be hydrogen bonding of the acetyl group at ring I (see Fig. 2) to a nearby amino acid; similar suggestions were made in Refs. [6,7,12].

Large differences between the hfc's of the non-methyl protons attached to rings II and IV were observed in the mutant and native dimers. They are attributed to differences in the conformations of rings II and IV of D_L and D_M relative to BChl a^+ in organic solvents.

The results on the heterodimer mutants were used to reinterpret and better understand the electronic structure of the native homodimer in *Rb. sphaeroides*. The direct assignments of hfc's to protons on the D_M and D_L halves of the homodimer was made possible by a comparison with the heterodimer results. The 2:1 asymmetry of D^+ in *Rb. sphaeroides* can be explained by the inequivalence of D_L and D_M found in the heterodimers. Comparison of spin densities at individual centers of π-spin density, using heterodimer hfc's as a monomeric reference, reveals that the wavefunction of the half in which the unpaired electron predominantly resides (i.e., D_L) has monomeric character, whereas the wavefunction of the other half (D_M) is more strongly perturbed by π–π interaction between the dimer halves. This is in accord with model calculations (see Appendix A of Ref. [11]) and points to an intradimer coupling that is stronger than had previously been assumed [12].

One of the motivations to investigate the electronic structure is to correlate it with electron transfer. An attempt was made to explain the preferential electron trans-

fer (unidirectionality) along the A-branch. From simple theoretical [20] considerations, one predicts that unidirectionality should be enhanced in the HL (M202) mutant and reduced and possibly reversed in the HL (L173) mutant. The lack of observed electron transfer along the B-branch in the HL (L173) mutant [14] is likely due to an oversimplification of the theory as discussed in the last section. The enhanced unidirectionality in the HL (M202) mutant was not determined since only limits of the electron transfer asymmetry were measured [14]. This suggests that a systematic study of the problem of unidirectionality would greatly benefit from an experimental determination of the values, rather than limits, of the asymmetry of electron transfer.

Acknowledgements

We thank M. Plato for many helpful discussions and suggestions concerning the interpretation of the data, K. Möbius for his help and encouragement, and Paul Beroza for help with the graphics. The work was supported by NIH GM 38254/48214 and NIH RCDA GM 00536 (C.S.), NSF MCB 94-16652 and NIH GM 13191 (G.F.) and by the Deutsche Forschungsgemeinschaft through a Forschungsstipendium (M.H.).

Appendix A. Determination of signs of hf tensor components

The elements of hf tensors in the crystallographic axis system (see Table 3) were obtained from a fit of the angular dependence of the hf couplings to Eq. (2). The tensors obtained are not diagonal because the principal axes of the hf tensors do not coincide with the crystallographic axes. To diagonalize the hf tensors (see Table 4) one needs to know, in addition to the absolute values, the signs of the hf tensor elements. While the signs of the diagonal tensor elements A_{ii} are obtained from Eq. 4 and general TRIPLE experiments, other criteria are needed to obtain the signs of the off-diagonal tensor elements (A_{ij}, $j \neq i$). In a related study [11], the signs of the off-diagonal elements were obtained by comparing the experimentally determined hf tensors with those obtained from MO calculations. To avoid the possibility of biasing the analysis towards the result of MO calculations, we used only methods based on experimental results.

There are 8 possible sign combinations for the three off-diagonal elements A_{ij} ($i, j = a, b, c$) of each tensor. Using all possible sign combinations eight tensors are obtained after diagonalization. They can be grouped into two sets of 4 tensors, each set representing the four sites in the unit cell belonging to the $P2_12_12_1$ space group. Within each set the four tensors have the same eigenvalues but different signs of the direction cosines. As an example, the tensor of the *1a* methyl protons in the HL (M202) mutant ($A_{iso} = 6.16$ MHz, see Table 2) yields the following sets of principal values:

$$\begin{array}{lll} \text{Set 1:} & A^{dip}_{xx} = -0.65\,\text{MHz} & \text{Set 2:} \quad A^{dip}_{xx} = -1.08\,\text{MHz} \\ & A^{dip}_{yy} = -0.54\,\text{MHz} & \qquad\quad A^{dip}_{yy} = +0.21\,\text{MHz} \\ & A^{dip}_{zz} = +1.20\,\text{MHz} & \qquad\quad A^{dip}_{zz} = +0.87\,\text{MHz} \end{array} \tag{12}$$

Set 1 is obtained by a sign combination of A_{ab}, A_{ac}, $A_{bc} > 0$, whereas Set 2 is the result of a diagonalization using $A_{ab} < 0$; A_{ac}, $A_{bc} > 0$. To decide which of these two sets corresponds to reality, we invoked the experimentally established axial symmetry of the hf tensor for methyl protons [16], i.e., $A_{xx} = A_{yy} = -1/2\ A_{zz}$. Set 1 is close to axial symmetry and was, therefore, chosen to be the right one. The tensor of Set 1 in Eq. (12) corresponds to one site. To obtain the other three tensors corresponding to the different sites, the signs of two off-diagonal tensor components have to be changed; this corresponds to a rotation of 180° about a principal axis [23]. The remaining task is to assign each tensor to a specific crystallographic site. To obtain the *relative* signs of the off-diagonal elements of different hf tensors, the magnetic field B_0 was set to a position (e.g., 45° from the crystal axis) where the two magnetically inequivalent sites give rise to two sets of lines. When an ENDOR transition belonging to one site is irradiated, only lines belonging to same site show intensity changes. This is shown, for example, for lines 1, 2, 4 and 6 of the HL (M202) mutant in the *bc*-plane (see Fig. 6a). All lines labeled with the same mark (circle or square) belong to the same site. The corresponding signs of A_{ij} are obtained from Eq. 3. To obtain the *absolute* signs, the signs of all three A_{ij} for *one* hf tensor are required. This was obtained for the methyl group hf tensor 6, in HL (M202), since for it the correlation between structure and tensor principal axes is most clearly defined (A_{zz}, the symmetry axis, points along the C_π–CH_3 bond direction) and the proper site is the one for which the angle between tensors axis and bond direction is smallest (see Table 5).

Appendix B. Hf tensor directions of non-methyl β protons

All major hf couplings in D^+ are due to β-protons; hence the analysis of the anisotropy of β-protons is crucial. For β-protons of rotating methyl groups the directions of the tensor axes are determined by the rotational symmetry as described in the section 'Assignment of hf couplings'. For non-methyl β-protons the relation of tensor directions to the molecular structure needs to be established. We follow the procedure of McConnell and Strathdee, who have calculated the dipole–dipole interaction of electron and nuclear spins in molecules with planar

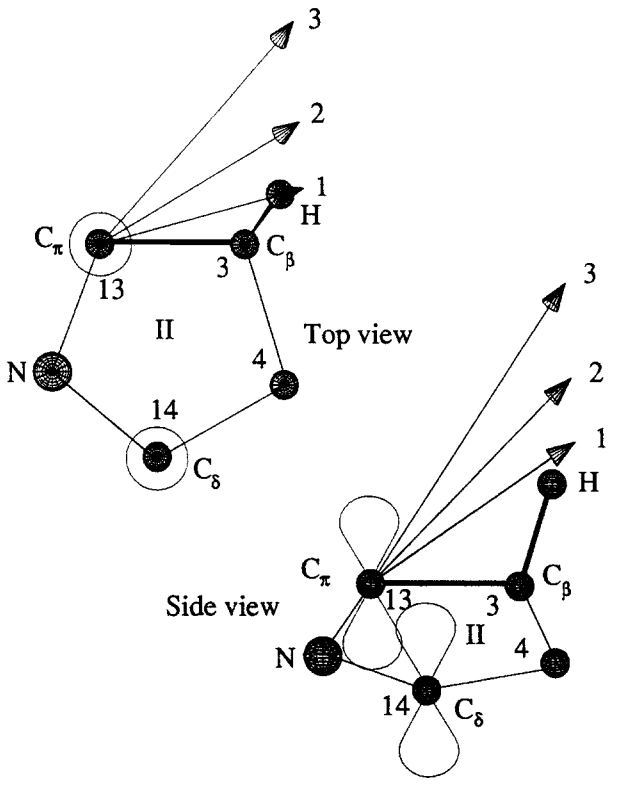

Fig. 11. Calculated direction of the principal axis, A_{zz}, of the hf tensor of proton at position 3 of pyrrole ring II of BChl a^+ (see Fig. 2). The calculation assumes a dihedral angle $\phi = 30°$ (see Appendix B). Arrows correspond to different spin densities ρ_δ at C_δ. They are: $\rho_\delta = 0$, Vector 1; $\rho_\delta = 0.5\ \rho_\pi$, Vector 2; $\rho_\delta = \rho_\pi$, Vector 3. Note that while increasing spin density at C_δ increases the deviation of the tensor axes from the C_π–H direction, the axes remain on the side of the pyrrole ring on which the proton is located.

π-systems [43]. In their calculation, Slater atomic orbitals are used for the $2s$ and $2p$ orbitals of carbon atoms, and the anisotropy is considered as a dipole–dipole interaction. In Ref. [43] only α-protons are explicitly dealt with.

To extend the analysis to β (non-methyl) protons, the analytical formula given in Ref. [43] was incorporated into a Fortran program by M. Plato (personal communication). We used it to calculate the dipole–dipole interaction in the C_π–C_β–H fragment (see Fig. 11) between the π-electron center located at C_π and the proton. Atomic coordinates are given by standard bond lengths and angles. Since the positions of the β-protons are not given in the X-ray structure (see section 'Assignment of non-methyl β-protons'), hf tensors were calculated for various dihedral angles ϕ (defined as in Eq. (6)) of the proton. For the angles investigated (ranging from $\phi = 0°$ to $\phi = 40°$) the tensor was axially symmetry ($\delta < 0.1$, see Eq. (5)) with the principal axis corresponding to the largest principal value (A_{zz}) within 10° of the C_π–H direction. This result is similar to that obtained for a *point-dipole* approximation in which A_{zz} is collinear with the C_π–H direction. These results are, however, in contradiction with experiments which showed that the hf tensors corresponding to lines 1 and 2 in the HL (M202) mutant are not axially symmetric ($\delta = 0.61$ and 0.54, respectively, see Table 4). We attribute this discrepancy to the presence of an additional π-center which for proton *3* is at position C14 (see Figs. 2 and 11). Calculating the dipole–dipole interaction for a proton under the influence of both π-centers leads to non-axially symmetric hf tensors with typical values of $\delta = 0.5$–0.6. The value of δ depends on the dihedral angle ϕ, since the distance of the proton to C_δ changes with ϕ. The orientations of the principal axes in the molecular framework are illustrated in Fig. 11 for $\phi = 30°$ and different values of the spin density ρ_δ. For $\rho_\delta = 0$ the direction is indicated by Vector 1; for $\rho_\delta = 0.5\ \rho_\pi$ by Vector 2 and for $\rho_\delta = \rho_\pi$ by Vector 3; the latter corresponds most closely to our situation as deduced from the similarities of the values of the hfc's at position *3* and *4* (lines 2 and 1) (see Tables 1 and 4). The deviation of the tensor axes from the C_π–H directions for the three cases are: 10°, 20°, and 30°, respectively. The corresponding values of the anisotropy parameter δ are: 0.1, 0.4 and 0.5.

In spite of the large deviation of the tensor axis from the C_π–H direction, the tensor directions can be used for the assignment, since in all cases the axes remain on the side of the nodal plane of the π-orbital, on which the proton is located (see Fig. 11). Consequently, the tensor directions can be used to discriminate between the protons at positions *3* and *4* in BChl *a*, since they are on opposite sides of that plane (see Fig. 2). The calculated principal axis, corresponding to the smallest tensor element, is perpendicular to the nodal plane of the π-electron system, which is in agreement with experiment (see Fig. 7).

Thus, there is qualitative agreement between experimental and calculated parameters. For a quantitative determination of the positions of the non-methyl β-protons, exact spin densities at the relevant π-centers are needed. Also, the method employed here neglects the effect of π-π and π-σ spin polarization, which are important, if puckering of the BChl *a* system occurs. Such effects are preferably treated using molecular orbital methods, e.g., the RHF-INDO/SP method developed by M. Plato et al. [12], which has recently been extended to include anisotropic hf interactions [11,12].

References

[1] Chang, C.-H., Tiede, D., Tang, J., Smith, U., Norris, J. and Schiffer, M. (1986) FEBS Lett. 205, 82–86.
[2] Allen, J.P., Feher, G., Yeates, T.O., Rees, D.C., Eisenberg, D.S., Deisenhofer, J., Michel, H. and Huber, R. (1986) Biophys. J. 49, 583a.
[3] Allen, J.P., Feher, G., Yeates, T.O., Rees, D.C., Deisenhofer, J., Michel, H. and Huber, R. (1986) Proc. Natl. Acad. Sci. USA 83, 8589–8593.
[4] Yeates, T.O., Komiya, H., Chirino, A., Rees, D.C., Allen, J.P. and Feher, G. (1988) Proc. Natl. Acad. Sci. USA 85, 7993–7997.
[5] Ermler, U., Fritzsch, G., Buchanan, S. and Michel, H. (1993) in: Research in Photosynthesis, Vol. I (Murata, N., ed.), p. 341–347, Kluwer, Dordrecht.

[6] Chang, C.-H., El-Kabbani, O., Tiede, D., Norris, J. and Schiffer, M. (1991) Biochemistry 30, 5352–5360.
[7] Ermler, U., Fritzsch, G., Buchanan, S.K. and Michel, H. (1994) Structure 2, 925–936.
[8] Feher, G., Hoff, A.J., Isaacson, R.A. and Ackerson, L.C. (1975) Ann. N.Y. Acad. Sci. 244, 239–259.
[9] Norris, J.R., Scheer, H. and Katz, J.J. (1975) Ann. N.Y. Acad. Sci. 244, 260–280.
[10] Plato, M. Möbius, K., Lubitz, W., Allen, J.P., Feher, G. (1990) in Perspectives in Photosynthesis (Jortner, J. and Pullman, P., eds.), pp. 423–434, Kluwer, Dordrecht.
[11] Lendzian, F., Huber, M., Isaacson, R.A., Endeward, B., Plato, M., Bönigk, B. Möbius, K., Lubitz, W. and Feher, G. (1993) Biochim. Biophys. Acta 1183, 139–160.
[12] Plato, M., Lendzian, F., Lubitz, W., Möbius, K. (1992) in: Structure, Function and Dynamics of the Bacterial Reaction Center (Breton, J. and Vermeglio, A., eds.), pp. 109–118, Plenum Press, New York.
[13] Bylina, E.J. and Youvan, D.C. (1988) Proc. Natl. Acad. Sci. USA 85, 7226–7230.
[14] McDowell, L.M., Gaul, D., Kirmaier, C., Holten, D. and Schenck, C.C. (1991) Biochemistry 30, 8315–8322.
[15] Chirino, A.J., Lous, E.J., Huber, M., Allen, J.P., Schenck, C.C., Paddock, M.L., Feher, G. and Rees, D.C. (1994) Biochemistry 33, 4584–4593.
[16] Huber, M., Lous, E.J., Isaacson, R.A., Feher, G., Gaul, D. and Schenck, C.C. (1990) in Reaction Centers of Photosynthetic Bacteria (Michel-Beyerle, M.-E., ed.), pp. 219–228, Springer, Berlin.
[17] Bylina, E.J., Kolaczkowski, S.V., Norris, J.R. and Youvan, D.C. (1990) Biochemistry 29, 6203–6210.
[18] Feher, G. (1992) J. Chem. Soc. Perkin Trans 2, 11, 1861–1874.
[19] Huber, M., Isaacson, R.A., Abresch, E.C., Feher, G., Gaul, D. and Schenck, C.C. (1992) Biophys. J. 61, A104, Abstr. 602.
[20] Plato, M., Möbius, K., Michel-Beyerle, M.-E., Bixon, M. and Jortner, J. (1988) J. Am. Chem. Soc. 110, 7279–7285.
[21] Paddock, M.L., Rongey, S.H., Feher, G. and Okamura, M.Y. (1989) Proc. Natl. Acad. Sci. USA 86, 6602–6606.
[22] Feher, G. and Okamura, M. (1978) in The Photosynthetic Bacteria (Clayton, R.K. and Sistrom, W.R., eds.), Ch. 19, p. 349–386, Plenum Press, New York.
[23] Isaacson, R.A., Lendzian, F., Abresch, E.C., Lubitz, W. and Feher, G. (1995) Biophys. J. 69, 311–322.
[24] Lubitz, W., Isaacson, R.A., Abresch, E.C. and Feher, G. (1984) Proc. Natl. Acad. Sci. USA 81, 7792–7796.
[25] Kajfez, D. and Guillon, P. (1986) Dielectric Resonators, Artech House.
[26] Lous, E.J., Huber, M., Isaacson, R.A. and Feher, G. (1990) in Reaction Centers of Photosynthetic Bacteria (Michel-Beyerle, M.E., ed.), pp. 45–55, Springer, Berlin.
[27] Lendzian, F., Endeward, B., Plato, M., Bumann, D., Lubitz, W. and Möbius, K. (1990) in Reaction Centers of Photosynthetic Bacteria (Michel-Beyerle, M.E., ed.), pp. 57–68, Springer, Berlin.
[28] Walsh, W.M. and Rupp, L.W. (1986) Rev. Sci. Instrum. 57, 2278–2279.
[29] Dykstra, R.W. and Markham, G.D. (1986) J. Mag. Res. 69, 350–355.
[30] Isaacson, R.A. (1976) Rev. Sci. Instrum. 47, 973–974.
[31] Tränkle, E. and Lendzian, F. (1989) J. Magn. Reson. 84, 537–547.
[32] McElroy, J.D., Feher, G. and Mauzerall, D.C. (1969) Biochim. Biophys. Acta 172, 180–183.
[33] Debus, R.J., Feher, G. and Okamura, M.Y. (1986) Biochemistry 25, 2276–2287.
[34] Debus, R.J., Feher, G. and Okamura, M.Y. (1985) Biochemistry 24, 2488–2500.
[35] Feher, G. (1958) Physica 24, 80–87.
[36] Dinse, K.P., Biehl, R. and Möbius, K. (1974) J. Chem. Phys. 61, 4335–4341.
[37] Cook, R.J. and Whiffen, D.H. (1964) Proc. Phys. Soc. 84, 845–848.
[38] Biehl, R., Plato, M. and Möbius, K. (1975) J. Chem. Phys. 63, 3515–3522.
[39] Feher, G., Isaacson, R.A., Okamura, M.Y. and Lubitz, W. (1985) in Antennas and Reaction Centers of Photosynthetic Bacteria – Structure, Interactions and Dynamics (Michel-Beyerle, M.-E., ed.), pp. 174–189, Springer, Berlin.
[40] Feher, G., Hoff, A.J., Isaacson, R.A. and Ackerson, L.C. (1975) Ann. N.Y. Acad. Sci. 244, 239–259.
[41] Gouterman, M. (1961) J. Mol. Spectrosc. 6, 138–163.
[42] Lubitz, W. (1991) in The Chlorophylls (Scheer, H., ed.), pp. 903–944, CRC Press, Boca Raton.
[43] McConnell, H.M. and Strathdee, J. (1959) Mol. Phys. 2, 129–138.
[44] Lendzian, F. (1982) PhD thesis, Free University Berlin.
[45] Fraenkel, G.K. (1967) J. Phys. Chem. 71, 139–171.
[46] Heller, C. and McConnell, H.M. (1960) J. Chem. Phys. 32, 1535–1539.
[47] Davis, M.S., Forman, A., Hanson, L.K., Thornber, J.P. and Fajer, J. (1979) J. Phys Chem. 83, 3325–3332.
[48] Hanson, L.K. (1991) in The Chlorophylls (Scheer, H., ed.), pp. 993–1014, CRC Press, Boca Raton.
[49] Plato, M., Traenkle, E., Lubitz, W., Lendzian, F. and Möbius, K. (1986) Chem. Phys. 107, 185–196.
[50] Rautter, J., Lendzian, F., Schulz, C., Fetsch, A., Kuhn, M., Lin, X., Williams, J.C., Allen, J. and Lubitz, W. (1995) Biochemistry 34, 8130–8143.
[51] Marcus, R.A. and Sutin, N. (1985) Biochim. Biophys. Acta 811, 265–322.
[52] Silbey, R., Jortner, J., Rice, S.A. and Vala, M.T. (1965) J. Chem. Phys. 42, 733 and J. Chem. Phys. 43, 2925–2926.
[53] Arlt, T., Schmidt, S., Kaiser, W., Lauterwasser, C., Meyer, M., Scheer, H. and Zinth, W. (1993) Proc. Natl. Acad. Sci. USA 90, 11757–11761.
[54] Pople, J.A. and Beveridge, D.L. (1970) Approximate Molecular Orbital Theory, pp. 128–129, McGraw-Hill, New York.
[55] Davis, D., Dong, A., Caughey, W. and Schenck, C. (1992) Biophys. J. 61, abstr. 876.
[56] Marcus, R. (1956) J. Chem. Phys. 24, 966–978.
[57] Laporte, L., McDowell, L.M., Kirmaier, C., Schenck, C.C. and Holten, D. (1993) Chem. Phys. 176, 615–629.
[58] Huber, M., Davis, D. and Schenck, C.C. (1995) Biophys. J. 68, A94 Abstr. M–Pos 383.
[59] Nabedryk, E., Allen, J.P., Taguchi, A.K.W., Williams, J.C., Woodbury, N.W. and Breton, J. (1993) Biochemistry 32, 13879–13885.